IMAGING THE MANTLE USING RECEIVER FUNCTIONS BENEATH SOUTHERN CALIFORNIA

by

JASON ERIC LEWIS, B.S.

A THESIS

IN

GEOSCIENCE

Submitted to the Graduate Faculty
of Texas Tech University in
Partial Fulfillment of
the Requirements for
the Degree of

MASTER OF SCIENCE

Approved

_____
Chairperson of the Committee

_____

_____

_____
Dean of the Graduate School

August, 2004

TABLE OF CONTENTS

ABSTRACT

Mantle convection in generally accepted as the driving mechanism for lithospheric plate motion. There is, however, a debate as to weather convection occurs in large cells involving the whole mantle or if there is layered convection in chemically stratified mantle. Thermal relationships and chemical composition hypothesized for the upper mantle based on these models will affect the depth to olivine and garnet phase changes differently. This study will use receiver functions to map short wavelength variations in the depths to these phase changes. In the past, earthquake seismology has lacked the data coverage to employ high resolution 3-D seismic reflection techniques typically employed by the oil industry. Southern California has twenty years of data from 22 permanent broadband seismic stations and, therefore, provides the richest data set for such analysis.

As waves pass through seismic discontinuities P to S conversions occur and Pds where d indicates the depth of conversion. For example the Pds conversion from the 410 km discontinuity (the hypothesized olivine to spinel transition) will be labeled P410s. These receiver functions are produced by deconvolving radial component seismograms with the vertical (assumed to be the P-wave signal) to isolate P-to-s conversion amplitudes as a function of time. To increase the signal to noise ratio and provide a 3-D image of the subsurface these receiver functions are back projected through a 3-D model and stacked by common conversion point (CCP) similar to the CMP method used in reflection seismology. Earlier work conducted by these investigators revealed horizons near the 670 km depth that were anti correlated in depth in a way that supports the presence of phase changes in both the olivine and garnet mineral systems. While the

depth variations between the 410 and 670 were consistent with the phase change in the olivine mineral system no evidence for the garnet system were observed at the 410 km discontinuity. This work revisits this earlier work using more than twice the volume of data to provide a higher resolution model of these upper mantle seismic boundaries.

LIST OF TABLES

LIST OF FIGURES

CHAPTER I

INTRODUCTION

Little is known about the 3-D structure of the upper mantle. The driving force behind plate tectonics is thought to be mantle convection, but there is some debate as to whether convection occurs as whole mantle convection in an isochemical mantle (Katsura and Ito, 1989) or in multiple cells in a layered mantle (Duffy and Anderson, 1989; Anderson, 1989; Gasparik, 1997). The lithosphere generally is believed to be the base of the stable part of continental plates, but recent work has supported the tectosphere hypothesis (Jordan, 1988) in which older continental regions have stable mantle to depths as great as 400 km. The relationship between crustal tectonic features and the upper mantle also is poorly understood. Recent work has called into question the depth of heat sources for the Yellowstone hotspot and the East Pacific Rise as it passes beneath southern California. Furthermore, recent models of the tectonics of southern California include small-scale delimitation of the lithosphere in what is essentially localized convection (Xie S., 2003; Trubitsyn et al., 2003). There is uncertainty as to how deep these features extend because of the tectonic complexity of southern California. This region has abundant seismic data, so it is an ideal location to study crust mantle interaction.

An understanding of the nature of the upper mantle transition zone is key to resolving many of these issues. The transition zone is located between 350 and 750 km

depth in an area where several mineral phase changes occur, producing a transition in mineralogy (Davis, 1999). Seismic discontinuities have been found and are thought to be the product of the mineralogical phase changes (Akaogi et.al., 1989). Therefore, whole mantle convection is possible, though not necessary. Others believe the discontinuities are due to chemical layering (Duffy and Anderson, 1989; Anderson, 1989; Gasparik, 1997). Because of the abundant data, southern California is a good location to study the transition zone. Receiver functions have become an important tool for studying the mantle and will be the primary tool employed in this study (e.g., Burdick and Langston, 1977; Langston, 1977, 1979, 1981, 1989; Owens et al., 1984, 1987, 1988; Owens and Crosson, 1988).

1.1 The Upper Mantle Transition Zone

The upper mantle transition zone is considered to be from about 350 to 750 km deep, with abrupt velocity increases near 410 and 660 km depths (Dziewonski and Anderson, 1981; Kennett and Engdahl, 1991). It is a region separating a peridotite-dominated mineralogy from a primarily denser region of perovskite structures (Figure 1.1). The 410 and 660 km observed discontinuities in the transition zone itself are thought to be due to a combination of olivine to spinel transformations and transformations of garnet into ilmenite and perovskite respectively (Simmons and Gurrola, 2000). These phase transforms may correlate to thermal anomalies in the mantle (Anderson, 1989). By mapping the depths to the thermal anomalies thermal anomaly

patterns can be determined. Methods for this comparison will be discussed in the section below.

1.2 Phase Transformations

High-pressure mineral physics laboratory experiments are preformed to determine temperatures and pressures where phase changes occur. The olivine transformations are attributed to an iso-chemical phase transformation where low-density (α) olivine transforms into a denser (β) spinel structure (Katsura and Ito, 1989) at pressures and temperatures consistent with those believed to exist near the 410 km discontinuity. Another transition is thought to exist when (β) spinel transforms into a denser (γ) spinel near the 520 km discontinuity (Shearer, 1990). At conditions near the 660 km discontinuity (γ) spinel dissociates into perovskite and magnesiowüstite (e.g., Ito and Takahashi, 1989) (Figure 1.2). If present, the 520 km discontinuity would have similar thermal properties as the 410 km, found by comparing the slopes of the discontinuities (Figure 1.2). However, there is about a 70 km range where the (β) Spinel and (γ) Spinel phases co-exist so the 520 km will produce a much smaller seismic response than the 410 or 660. The 410 km also has a 10 km zone of mixing of (α) olivine to (β)spinel, which will make it only recognizable in larger wavelengths than the 660.

The garnet mineralogical system may be another important component when considering the transition zone discontinuities (Gasparik, 1997). Garnet transforms into ilmenate and perovskite structures at temperatures and pressures near the same depths as the olivine components (Vacher et al., 1998). The combined olivine-garnet system along with their phase boundaries is shown in Figure 1.3. The 410 and 520 are about the same

in Figure 1.3 as in Figure 1.2, but the 660 is very different. This is because both the 410 and 520 are endothermic, as is the garnet phase changes. The 660 is exothermic, while the garnet phase change is endothermic. This will lower the depth to the phase change.

Temperature anomalies in the mantle can be detected by determining the thickness of the transition zone and topography of the various discontinuities. Clapeyron slopes (Equation 1.1) are used to describe the temperature and pressure, which is directly proportional to depth, conditions required for a phase transformation, such as:

$$(\zeta_d = Pd / dT). \qquad (1.1)$$

The Clapeyron slope is the derivative of pressure with respect to temperature. The subscript *d* represents the approximate transformation depth. Positive Clapeyron slopes indicate exothermic phase transformations and result in a shallowing of the mantle boundaries in cold regions such as subduction zones. Negative Clapeyron slopes indicate endothermic transformations and often result in a shallowing of the mantle transformation boundaries in warm regions such as thermal upwelligs (Figure 1.4). By combining these two transformations, the transition zones would thin in warmer areas and thicken in cooler areas.

1.3 Mantle Convection

King (1994) and Davis (1999) summarize the implications of the upper mantle transition zone in mantle dynamics. Temperatures and pressures control convection in the mantle by inducing as well as preventing it. Phase transforms with a positive Clapeyron slope (exothermic) assist convection since the material at downwelling regions

convert to a denser substance and will sink. This negative Clapeyron slope phase transform will act to stop upwellings by creating more dense material resisting upward motion. Phase transformations with negative slopes (endothermic) will inhibit mantle flow because the subducting material is converting to a less dense form and becoming more buoyant. In areas of upwelling, the more buoyant material will raise faster helping convection, but at the boundary, on the way up, it goes from low density to high; and so, it impedes convection. The 410-km discontinuity is thought to assist in mantle convection due to its positive Clapeyron slope, while the 660-km discontinuity inhibits mantle convection (Simmons and Gurrola, 2000). To illustrate this point, consider a slab approaching a transformation boundary with a positive Clapeyron slope. The slab is forced down as it transforms into a denser structure creating the beginnings of a convective cycle. A slab approaching a boundary with a negative Clapeyron slope will revert to a less dense structure. This density change will inhibit the slab from penetrating the boundary due to a local buoyancy effect. If the negative Clapeyron slope is steep enough, convection can be completely stopped. The density change at the 660 also will inhibit the slab from rising, and it could, theoretically, come to rest at the boundary. Sinking at the 410 and buoyancy at the 660 km discontinuity would produce small-scale convection and inhibit hole mantle convection. If a hot mantle plume is raising through the mantle transition zone, the material will become denser at the 660 km and slow rate of assent. If the material rises to the 410, it will become less dense and begin to rise faster. This also is conducive to small-scale convection within the mantle transition zone itself and would act to inhibit whole mantle convection.

1.4 Tectonic History of Southern California

Southern California has a long history of active tectonics creating a very complex continental margin (Figure 1.5). Before the Late Jurassic, several subduction and collision sequences occurred. These sequences resulted in terrain captures while consuming oceanic plates (Moores and Twiss, 1995; Ingersoll, 1998). During the Late Jurassic an oceanic arc complex collided with western North America causing the Nevadan orogeny (Moores and Twiss, 1995; Ingersoll, 1998). Subduction of the Farallon oceanic plate began soon after and continued through the Cretaceous producing an arc-trench system (Schweickert and Cowan, 1975). To the west is the Coastal Ranges which represents the accretionary prism (Dickenson, 1970). To the east is the fore-arc basin called the Great Valley (Dickenson, 1970). The magmatic arc is located east of the great valley is called the Sierra Nevadas (Dickenson, 1970; Saleeby, 1981). During the Eocene the Farallon plate started to subduct more rapidly (Coney, 1976; Dickinson and Snyder, 1978; Bird, 1984, 1988; Engebretson et al., 1985; Cross, 1986; Spencer, 1996). Due to the buoyancy of the slab it began a period of "flat-slab" subduction beneath the North American plate. This process is thought to quicken the progress of the Cretaceous Laramide orogeny. (Engebretson and Thompson, 1984).

During Neogene time the Farallon slab began subducting at a stepper angle as the East Pacific Rise approached the North American plate (Atwater, 1970). A dextral transform margin along the San Andreas Fault system was created as the Farallon plate was totally consumed (Atwater, 1970). This dextral motion eventually generated oblique

rifts in the Gulf of California where there is active spreading and it appears to continue today (Sedlock, 2003). Currently the San Andreas Fault is migrating westward as the pacific plate rotates toward the northwest (Atwater, 1970). The Salton Trough lies on the plate boundary separating the Pacific and North American plates, and is the southern terminus of the San Andreas Fault. The trough is the northern on land extension of the Gulf of California spreading system and is believed to be a pull-apart basin, which began opening at 4.5 Ma. (Larson et al., 1968; Moore and Buffington, 1968; Elders et al., 1972). To the north of the Salton Trough and South of the Garlock Fault is the Mojave Desert. It is an early Miocene northeast-southwest directed crustal extension zone. (Cheadle et al., 1986)

It has been proposed that small convection cells, resembling spreading centers or continental rift zones, are created as asthenophere rises into areas behind the trailing edge of the Farallon plate (Stewart, 1977). These areas called "slab windows" are produced as the Farallon plate subducts in conjunction with its own transform motion, creating areas lacking subducted oceanic material (Atwater and Stock, 1998). It is unclear if these processes affect the structure or composition of the upper mantle transition zone. Identifying relationships between the issues mentioned in this section and the mantle transition zone will be the focus of this thesis.

1.5 Seismic Data from Permanent Broadband Stations

Data from 22 seismic stations were obtained from the Incorporated Research Institute for Seismology (IRIS) through the Data Management Center (DMC) coordinated

by the University of Washington in Seattle. All stations (Table 1.1) in southern California and western Arizona were used in this study. All data from 1977 to June 2003 was gathered. All events with a magnitude of 5.5 and greater were screened for usable events. Only those that had clear P-wave arrivals were processed. The data was sorted for overall quality first by comparing the quality of signal to amount of noise. Then a visual inspection of each three-component seismogram with various bandpass filters was applied (0.02 Hz through 2 Hz). This was done to remove noise outside the frequency band that is significant to receiver function analysis of the upper mantle. Additional low pass filters were applied to remove signal generated scattering from crustal structures that often masks P410s and P660s phases. Approximately 3,000 seismograms were found. Since only half this amount is need, a second cut was made to keep only the best looking data. Between 800 and 1,500 three-component seismograms were kept at each frequency after all inspections.

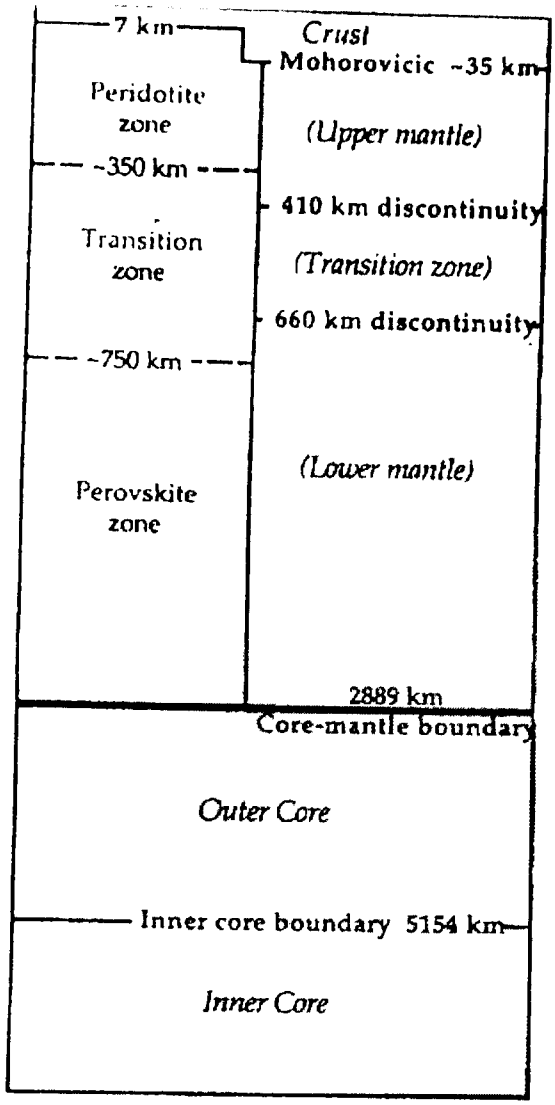

Figure 1.1. Components Defining the Upper Mantle Transition Zone.
Source: Taken directly from Davis (1999)

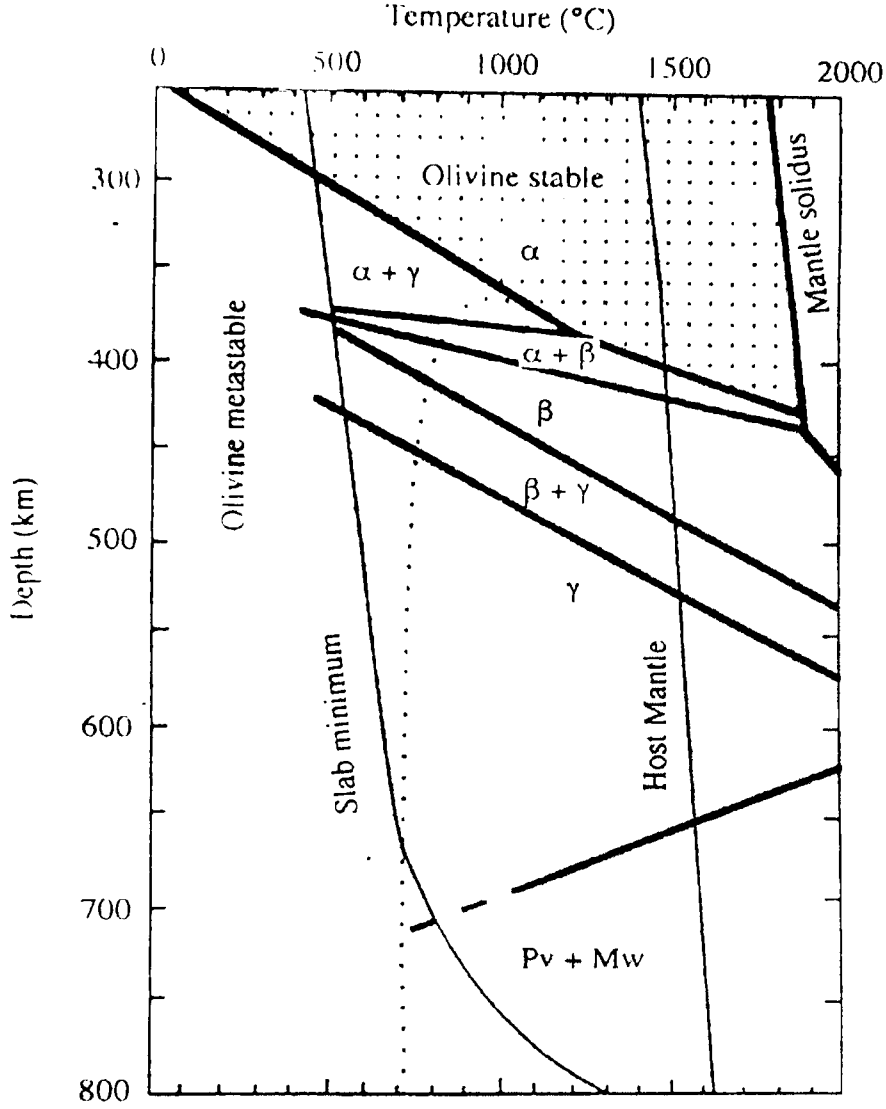

Figure 1.2. Stability Fields for Olivine Component Transformations.
Source: Edited from Akaogi et al (1989).

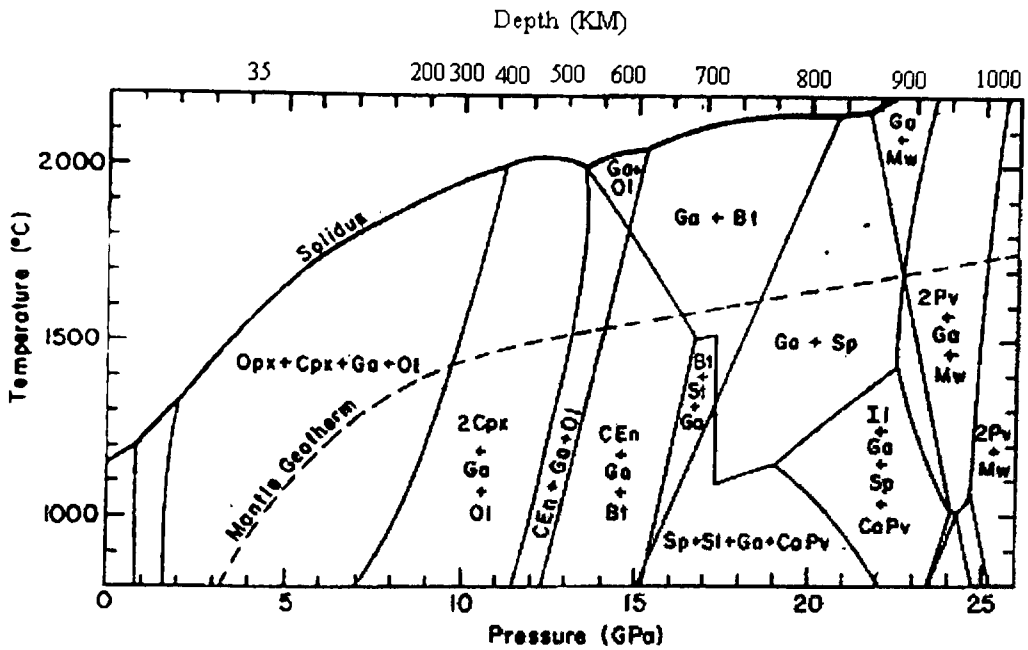

Figure 1.3. Transformation Boundaries for a Mixed Olivine/Garnet System.
"Ol" is olivine, "Ga" is garnet; "Bt" is β-spinel; "Sp" is γ-spinel; "Ill" is ilmenite; "Pv" is Perovskite; "Mw" is magnesiowüstite.
Source: Adapted from Gasparik (1997)

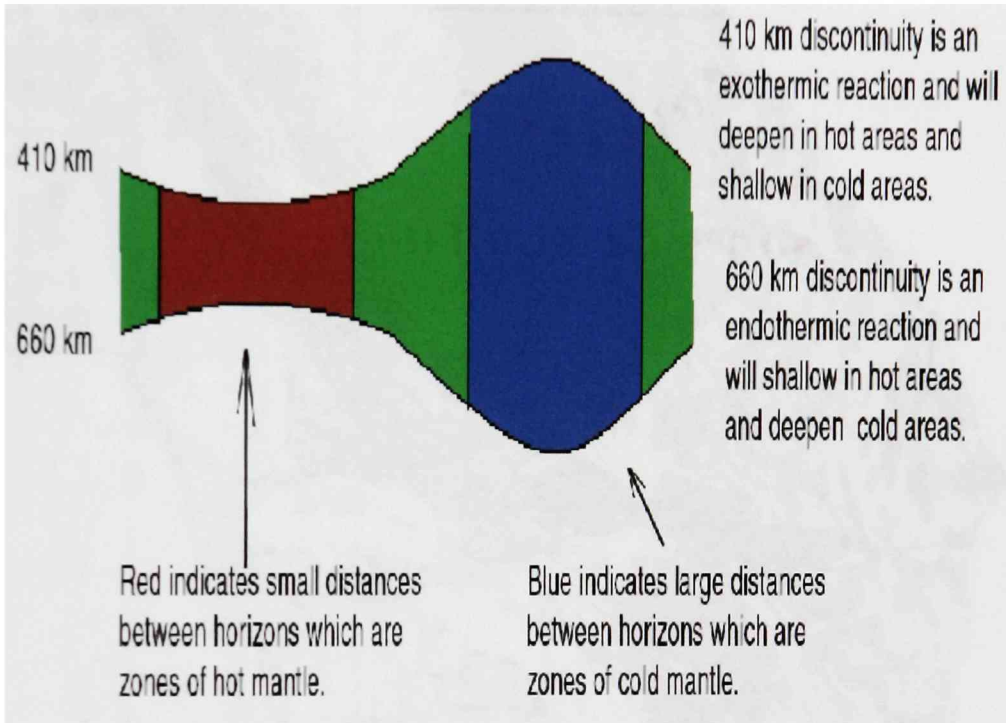

Figure 1.4. Discontinuities and their reactions to thermal conditions

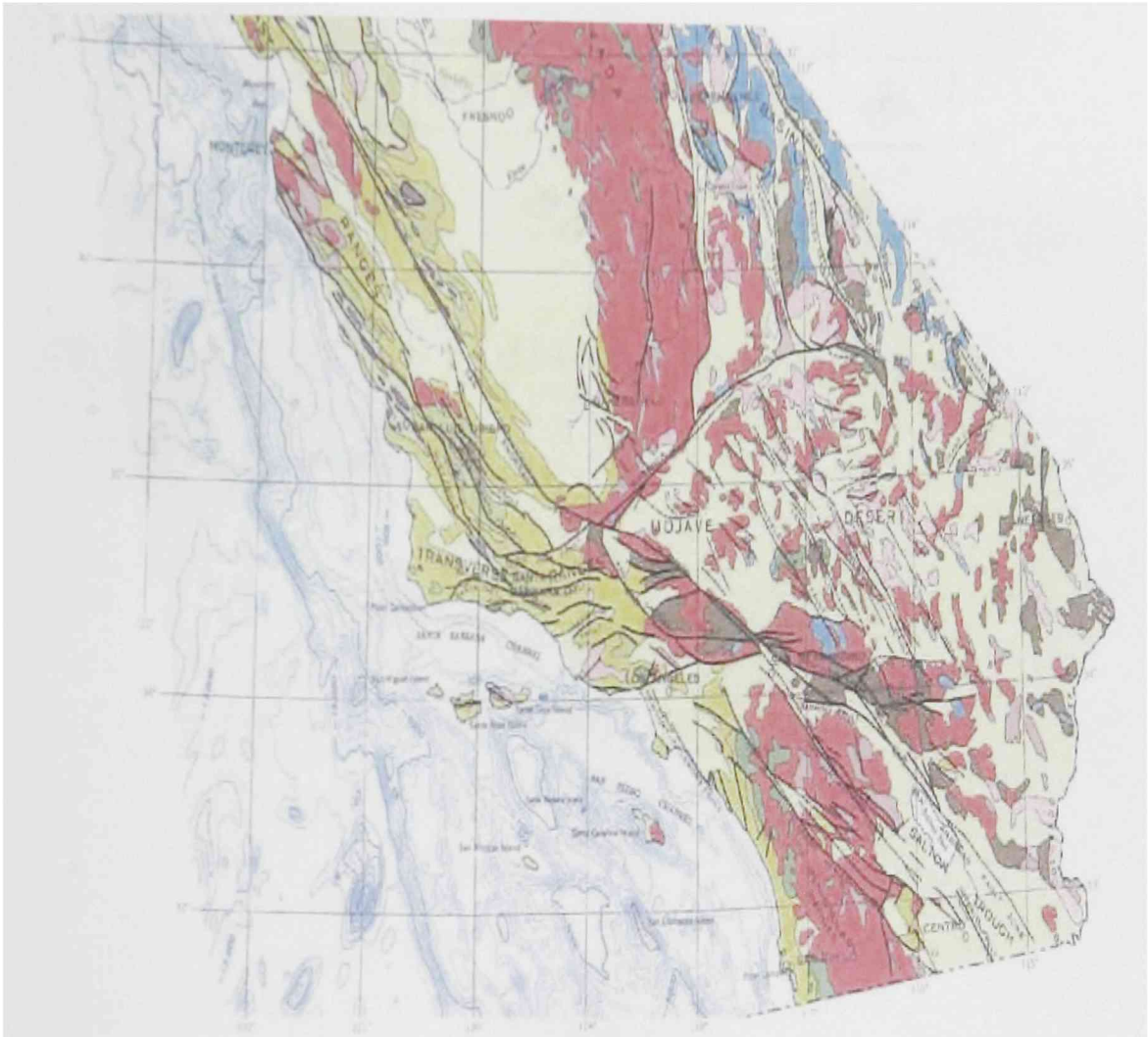

(a)

Figure 1.5. Geologic map of southern California.
(a) Map
(b) Key
Source: California Department of Conservation (2002)

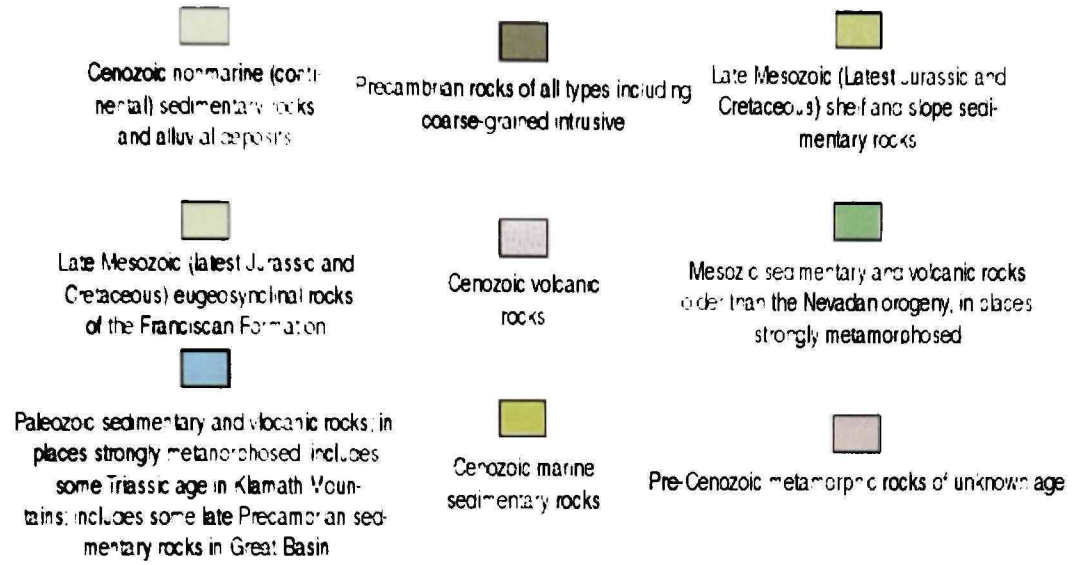

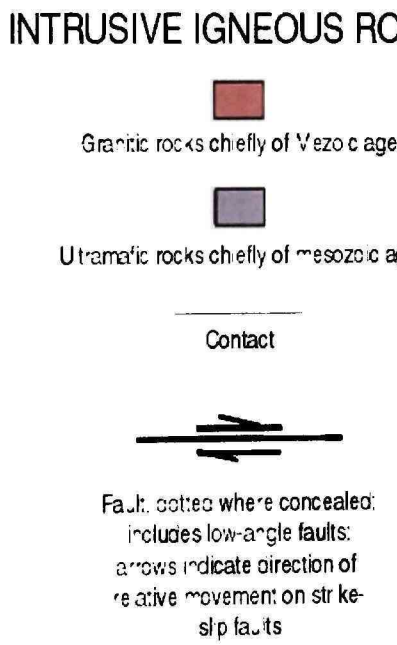

(b)
Figure 1.5. Continued
Source: California Department of Conservation

Table 1.1. Table of all stations used and their abbreviations
Also shown is the latitude, longitude and elevation of each station.

Table 1.1

Name	Abbreviation	Lat in Deg North	Long in Deg West	Elev (meters)
Barrett Dam	Bar	32.6	-116.6	548
Calabasas	Calb	34.1	-118.6	0
Columbia College	Cmb	38	-120.3	719
Cottonwood Creek	Cwc	36.4	-118	1553
Domenigoni Valley	Dgr	33.6	-117	700
Glamis	Gla	33	-114.8	627
China Lake	Gpo	35.6	-117.6	735
Goldston	Gsc	35.3	-116.8	990
Isabella	Isa	35.6	-118.4	835
Jamestown	Jas	37.9	-120.4	457
Mammoth Lakes	Mlac	37.6	-118.8	2170
Needles	Nee	34.8	-114.5	139
Osito Adit	Osi	34.6	-118.7	706
Pasadena	Pas	34.1	-118.1	295
Pinon Flat	Pas	33.6	-116.4	1280
Rancho Palos	Rpv	33.7	-118.4	115
Santa Barbara	Sbc	34.4	-119.7	90
San Nicolas	Sncc	33.2	-119.5	227
Seven Oaks Dam	Svd	34.1	-117	600
Tucson	Tuc	32.2	-110.7	874
USC, Los Angeles	Usc	34	-118.2	60
Victorville	Vtv	34.5	-117.3	847

CHAPTER II

SEISMIC TRAVEL TIME AND RECEIVER FUNCTIONS

The initial partial motion of an earthquake is parallel to the direction of wave propagation. This parallel motion or "P" wave is the first wave to contact the receiver and leave a trace. As the wave contacts a horizon of differing densities some of the parallel particle motion is transferred to perpendicular partial motion. This perpendicular partial motion is called an "S" wave. The contact between two horizons of differing densities is said to produce a "P-to-S" conversion. After the initial arrival of the P-wave at the receiver the P-to-S wave will arrive. The difference in arrival times of the "P" and "P-to-S" waves is called the delay time and is directly related to the depth and velocity to the horizon that created the P-to-S conversion.

Receiver function analysis uses seismic delay times from converted seismic phases. Depths to P-to-S conversions are recorded in the time domain but must be converted to the depth domain to produce the receiver functions. The locations of the P-to-S conversions in a 3-D study are determined by computing the unique ray path geometries of each receiver function through the 3-D model. Once the ray path geometry is known the position of each receiver function within the study area allows for stacking about geographical nodes.

2.1 Seismic Travel Times Theory

Determining travel times and ray paths for a given velocity model is a complex procedure. It requires differential travel time and range increments, for known velocities of rock units in the subsurface. The velocity model is defined in terms of slowness (equation 2.1) in a media rather than that of velocity (v), because travel time is the product of layer thickness multiplied by slowness.

$$u(z) = v^{-1}(z) \tag{2.1}$$

Where z is model depth. When considering the concepts of slowness we must first consider Snell's Law:

$$u_h = p = \frac{\sin\theta}{v(z)} = u\sin\theta \tag{2.2}$$

and then vertical slowness can be determined:

$$u_v = q(p,z) = (u^2(z) - p^2)^{\frac{1}{2}} = u\cos\theta \tag{2.3}$$

where subscripts h and v refer to horizontal and vertical slowness, respectively. P is the ray parameter or horizontal slowness (defined by Snell's law) and θ is the angle between the ray path angle and a line perpendicular to interface. When $u_v = 0$ or $u = p$ a ray reaches its turning point. In a particular velocity model layer the travel time and range can be obtained using the relationship of distance and time where $t = ud$. Using a ray

path angle, θ, the ray path length (d) through a layer (interval denoted as dz) is written as:

$$d = \frac{dz}{\sin\theta} = \frac{dz}{q\,u} = \frac{udz}{q} \tag{2.4}$$

where slowness components, q and u were used to determine $\sin\theta$. Travel time through dz becomes:

$$t = ud = \frac{u^2 dz}{q} \tag{2.5}$$

An arc length along the surface of the Earth can be determined using horizontal slowness in terms of p and q. Using θ and the components in equations (2.4) and (2.5), the equation for arc distances is as follows:

$$x = d\cos\theta = dz\frac{\cos\theta}{\sin\theta} = \frac{dz}{\tan\theta} = \frac{pdz}{q} \quad . \tag{2.6}$$

Where the vertical and horizontal components of slowness are employed. Travel time and arc distance are determined by integrating t and x over the entire ray paths:

$$T(p) = \int \frac{u^2(z)}{q(p,z)} dz \tag{2.7}$$

And

$$X(p) = \int \frac{p}{q(p,z)} dz \quad . \tag{2.8}$$

Where $T(p)$ and $X(p)$ are total travel time and arc distance as a function of ray parameter used first by Buland and Chapman (1983).

Transforming equations (2.7) and (2.8) into flat coordinates using the earth-flattening transformations gives the matrices below for differential time and range, after integration, in each model layer:

$$\Delta T_{ij} = \frac{dz_i}{\ln(\frac{u_i}{u_{i+1}})}\left\{(u_i^2 - p_j^2)^{\frac{1}{2}} - (u_{i+1}^2 - p_j^2)^{\frac{1}{2}}\right\} \qquad (2.9)$$

And

$$\Delta X_{ij} = \frac{dz_i}{\ln(\frac{u_i}{u_{i+1}})}\left\{\cos^{-1}\left(\frac{P_j}{u_i}\right) - \cos^{-1}\left(\frac{p_j}{u_{i+1}}\right)\right\}. \qquad (2.10)$$

Where i and j represent model sample number and ray parameter indices respectively. Velocity model thickness ($dz_i = |z_i - z_{i+1}|$) is bounded by u_i and u_{i+1} where $u_i > u_{i+1}$.

P waves and S waves have the same ray parameters as discussed above but different vertical slownesses. The incoming P phase is a direct arrival and does not cross any horizons and the P-to-S converted phase passed through the horizon of interest. The difference in time between the two phases (or delay time) represents the travel time from the horizon and the station. Using the arc distance (X) and back azimuth the ray can be traced back to its source in latitude, longitude and depth.

2.2 Receiver Functions

The transition zone discontinuities and the Moho can be imaged using compressional-to-shear conversions (denoted as Pds, where d is the P-to-S conversion depth beneath the surface) to model the depths to velocity interfaces (Langston, 1979). P-to-S conversion amplitudes are represented as receiver functions, and are computed as P-wave arrivals, which can be used to determine the depths of interfaces where compressional-to-shear wave conversions occur.

The particle motion of a P-wave is parallel to the direction of propagation and for near vertical angles of incidence it will be recorded on the vertical component of the seismogram (top Figure 2.2). When a P-wave crosses a horizon with significant velocity contrast P-to-S phases (Ps) are created (Figure 2.2). The particle motion of the S-wave is perpendicular to wave propagation, and will therefore, be recorded primarily on the horizontal components of the seismogram (middle trace of Figure 2.1). The traces are normalized and the P-wave on the middle trace is 1/3 the size of that on top trace. The horizontal components of the seismogram are used to create a radial component which records vertical S-phase information. The tangential component contains noise and is used to remove receiver functions with to much noise. This is done by comparing it to the horizontal component, which contains signal. The vertical and horizontal components are used (as described below) to create the receiver function.

Typically receiver functions are computed from P-wave arrivals. Events with magnitudes below 6.0 rarely produce useable receiver functions. For multiple station studies, receiver functions are back projected along their ray paths so Ps phases from

different stations can be stacked into one coherent image. This will not only remove problems with random incoherent noise but also will reduce signal generated noise (i.e. scattering from unresolvable 3-D structures in the crust). Three-dimensional images of discontinuities in the upper mantle can be created using this method.

2.2.1 Past Studies

Receiver functions have provided information about discontinuities in shallow earth structure and the crust mantle boundary using P-to-S conversions. Historically receiver functions were employed primarily for crustal work and occasionally to lithospheric work (Owes et al., 1984; 1988; Langtons et al., 1977; 1979). With greater deployment of 3-D broad band stations and networks investigations have extended into the transition zone (Vinnik, 1977; Gurrola, 1995) and with the deployment of closely spaced 3-D seismic stations along profiles 2-D images using common conversion point stacking (similar to reflection common midpoint stacking) have been produced (Dueker, 1997; 1998). Recent uses of 3D common conversion point stacking techniques have enriched data sets providing a much higher resolution image than ever possible before (Owens et al., 2000; Simmon and Gurrola, 2000).

2.2.2 Receiver Function Methods

A frequency domain procedure is used to remove compressional source function from the horizontal components of the seismogram (Langston, 1979). The expected component responses from an incoming P-wave are represented theoretically as:

$$D_V(t) = I(t) * S(t) * E_V(t)$$

$$D_R(t) = I(t) * S(t) * E_R(t) \qquad (2.11)$$

$$D_T(t) = I(t) * S(t) * E_T(t) \ .$$

Where V, R, T represent vertical, radial, and tangential components, respectively (Figure 2.1). I(t) is the instrument response and S(t) is the source function. E(t) is the earth response function and subscripted to denote a different response function in each direction. D(t) are the different components of the seismogram produced after convolution (represented by the asterisk). Typically in receiver function studies I(t) is assumed to be the same for all three components. Because of the steep angle of incidence the majority of the vertical component motion is P-wave energy and, therefore, Ev is assumed to be identical to the vertical component of the seismogram (Owens et al, 1984; Ammon 1991). The horizontal components can then be written as:

$$D_H(t) \approx E_V(t) * E_H(t) \qquad (2.12)$$

Where H is the horizontal component (either radial or tangential). The radial earth response function or $E_H(t)$ is called the receiver function and is given as:

$$E_H(t) = \Im^{-1}\left\{D_H(\omega) D_V(\omega)^* G(\omega)/\varphi(\omega)\right\} \qquad (2.13)$$

where $\Im^{-1}$ represents the inverse Fourier transform function, $G(\omega)$ represents a frequency domain Gaussian filter and $D_1(\omega)^*$ represents a complex conjugate of $D_1(\omega)$. $\varphi(\omega)$ is Dv times Dv' or for frequencies where this product is too small the value is replaced by a minimal value so as to avoid causing a singularity by dividing by very small numbers in the frequency domain (this is the equivalent to replacing small values with white noise).

2.3 Creating 3D Model

Time-domain receiver functions are converted to the depth domain by ray tracing through a 3D velocity model for the appropriate ray path geometry (Buland and Chapman 1983). This velocity model is based on Kennett and Engdahl's (1991) *iasp91* standard spherical Earth model. It is used to approximate incoming ray path geometries. The *NA95* 3-D velocity model is used for determining velocities of rock layers underneath North America (Van der lee and Nolet, 1997). Receiver functions are then Gaussian filtered to further remove noise. For regional interpretation of 3D Earth structure receiver functions are stacked to improve signal strength. Grids with regularly spaced nodes are placed over the study area. Receiver functions are assumed to be Ps phases and are back projected to latitude, longitude and depth through a 3-D velocity model (Figure 2.3).

To get a coherent stack of data many events and stations are needed. To produce a coherent image the data is stacked into bins as follows:

(1) Each event is back traced in time through to the appropriate latitude longitude and depth.

(2) Regularly spaced node points are place every .2 latitude and longitudes

(3) A cylindrical bin is defined around each node.

(4) The bin radius is increased until an appropriate number of receiver functions and an appropriate number of stations are included. If search radii are allowed to grow to large three-dimensional structure will be destroyed and horizons will be flattened.

(5) Once the limit of number of stations and receiver functions is found or the maximum radius is reached all data in the bin is stacked around the node (Figure 2.4).

The bin radius is plotted in the background of the seismic image as an indicator of resolution (Figure 2.5). Resolution will increase as the bin size is reduced. Noise is reduced as the number of traces per bin is increased. Several different stacking parameters were tested to determine optimal tradeoff between lateral coherency and resolution of topography on an interface while creating the 3D images.

The stacking parameters are listed on the top of each image (Figure 2.3, 3.1, 3.2, 3.5, 3.6, 3.7). For example in Figure (2.3) the top can be read as:

Minimum number of contributing stations per node:	4
Minimum number of traces per node:	50
Maximum search radius about a node:	1.0°
Sample increment (node spacing = dz):	2.5°

By increasing the number of stations and receiver functions used the image is easier to interpret by producing more coherent signal but resolution is sacrificed where large bins are required.

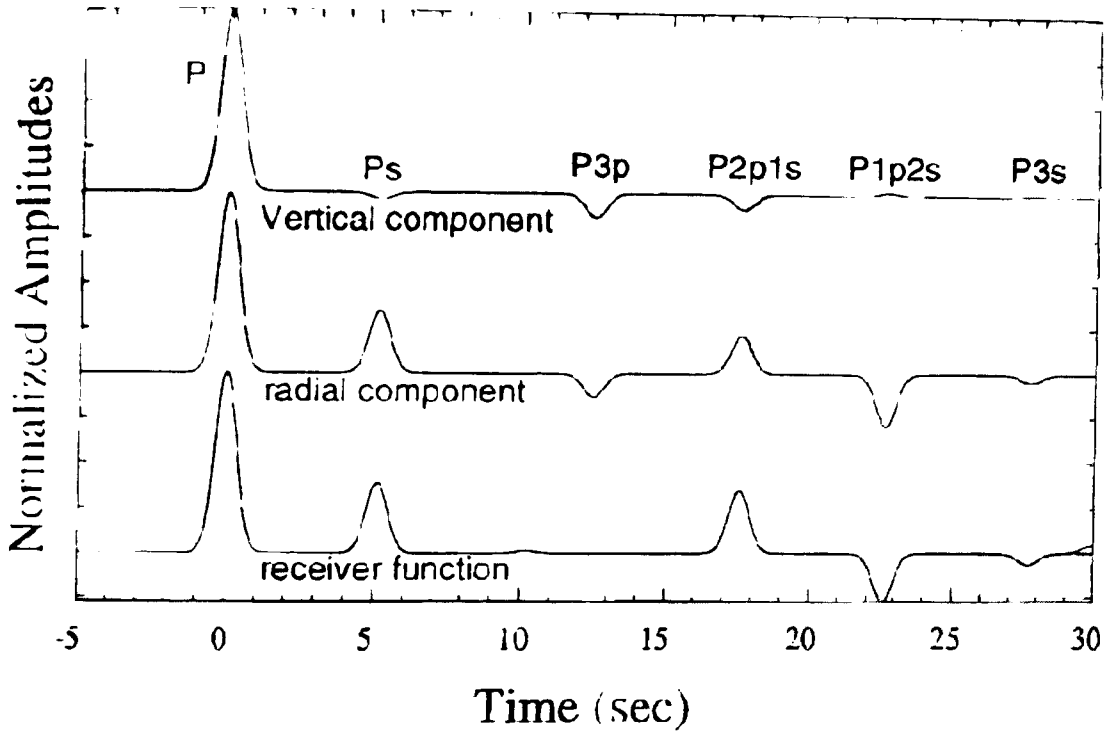

Figure 2.1. Synthetic seismograms and radial component
The receiver function computed for the layer over a half space given in the upper left hand corner of figure (2.2). The vertical component is assumed to be the source function and composed of the P-waves. The receiver function is computed by deconvolving the vertical from the horizontal to isolate P-to-s conversions.
Source: Gurrola (1995)

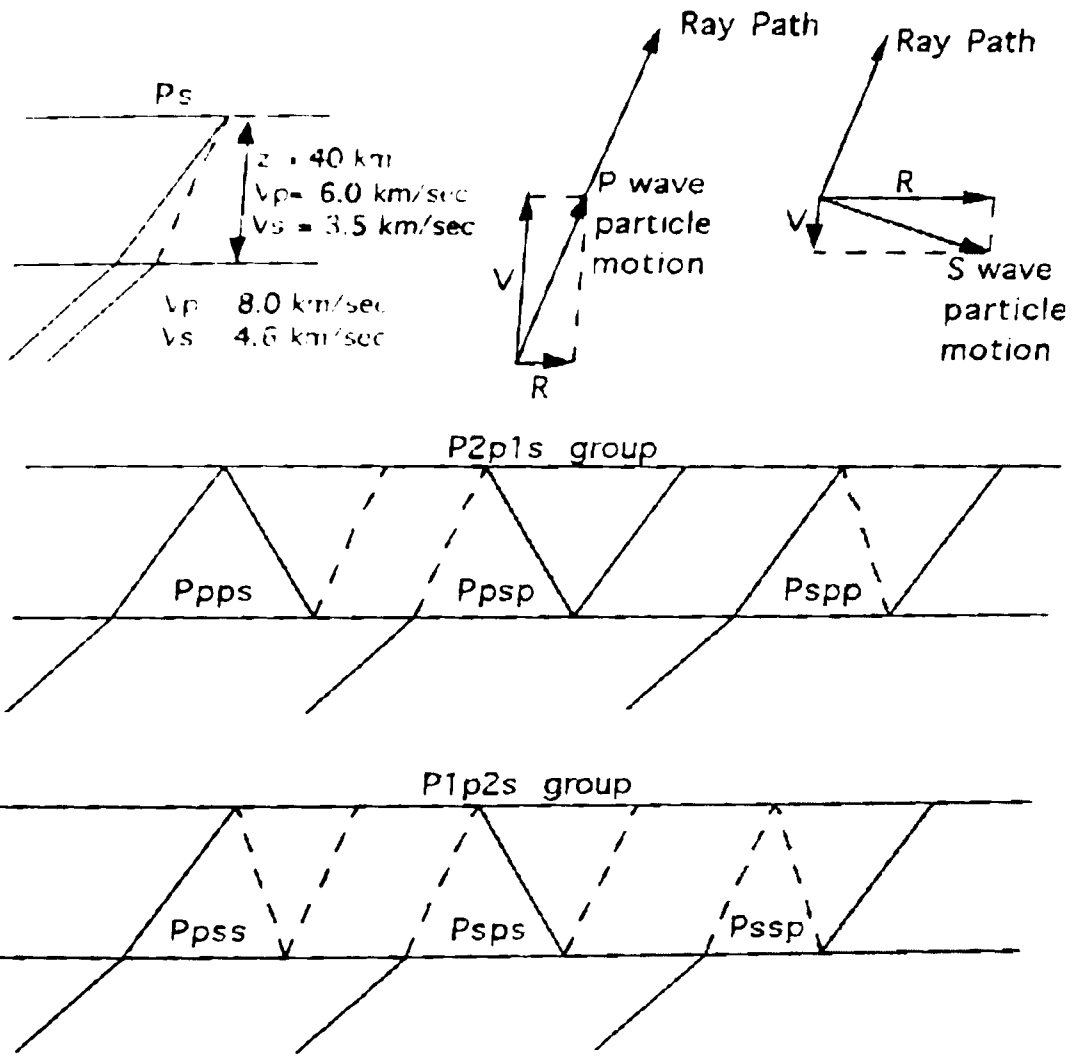

Figure 2.2. Geometrys of phases present on figure (2.1).
Dashed lines represent S phases and solid lines are used to indicate P phases. The model used to compute the synthetic seismograms and receiver functions in figure (2.1) are shown on the upper left corner. On the upper right of this figure are particle notion diagrams of the P phase (middle) and converted S phase (right).
Source: Gurrola (1995)

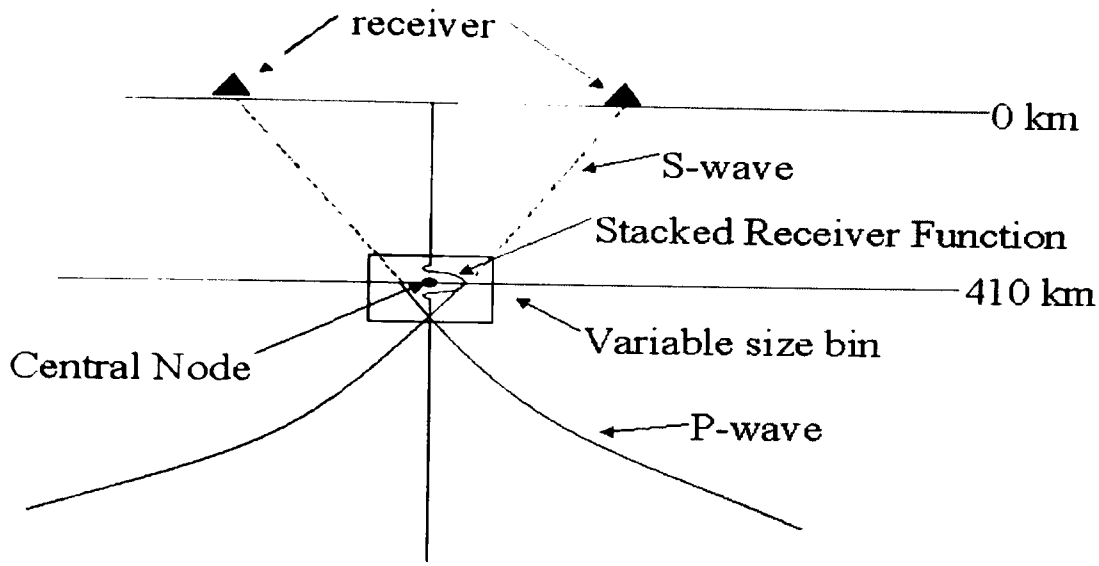

Figure 2.3. Figure depicting wave geometries, and central node. Receiver functions are stacked inside the bin around the node.

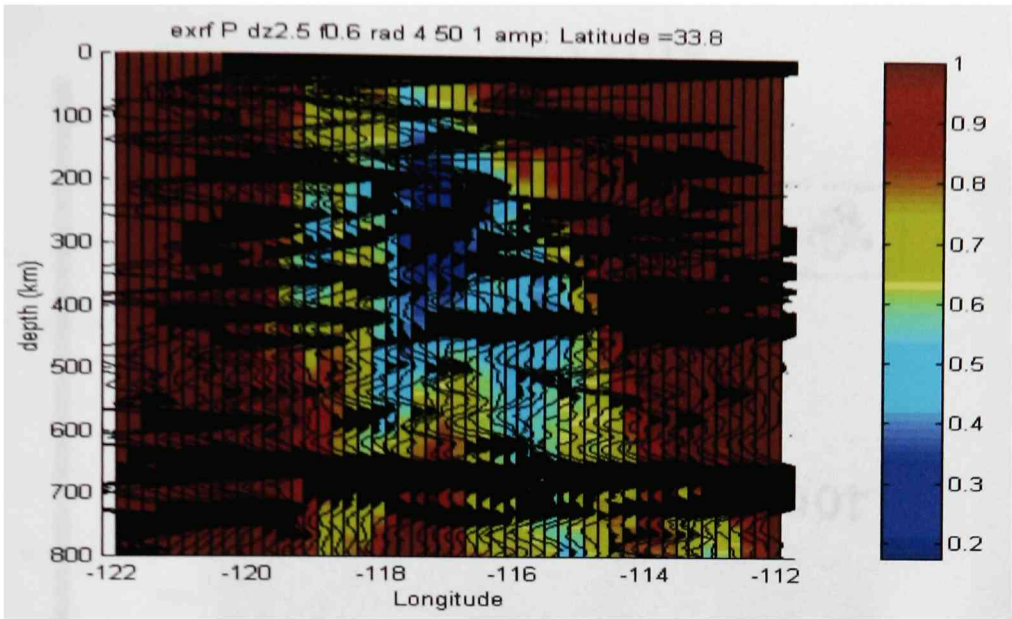

(a)

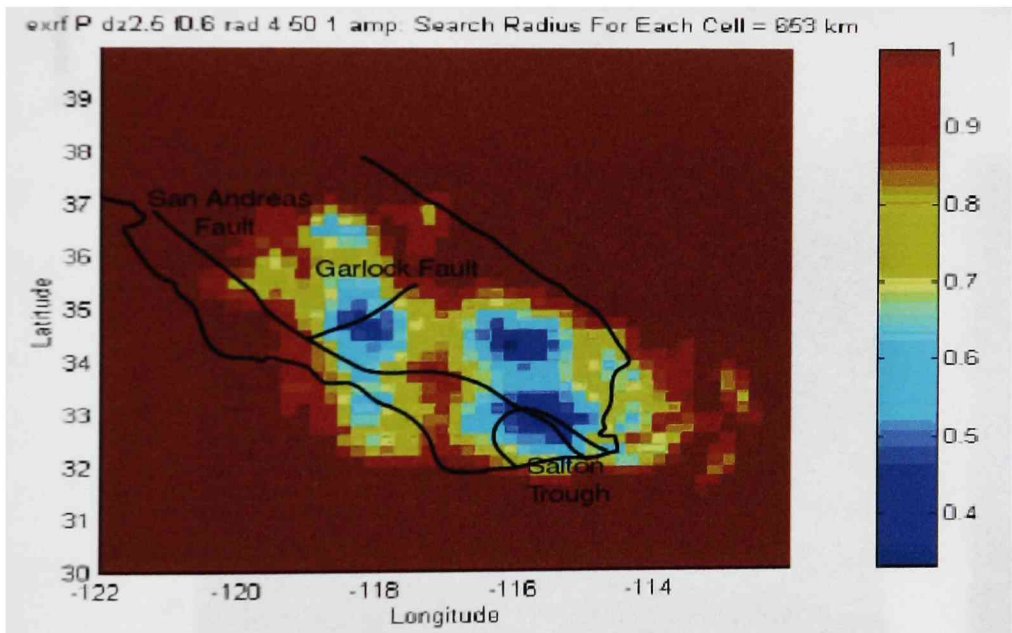

(b)

Figure 2.4. Figures depicting search radius throughout study area.
(a) is a vertical view taken a 33.8° Latitude. (b) view is a horizon at 653 km depth. Colors represent distance in degrees of latitude and longitude searched before a minimum number of traces were found. The minimum number of traces and maximum search radius is found in the information above the figure. Number of traces: 50, Maximum search radius: 1°

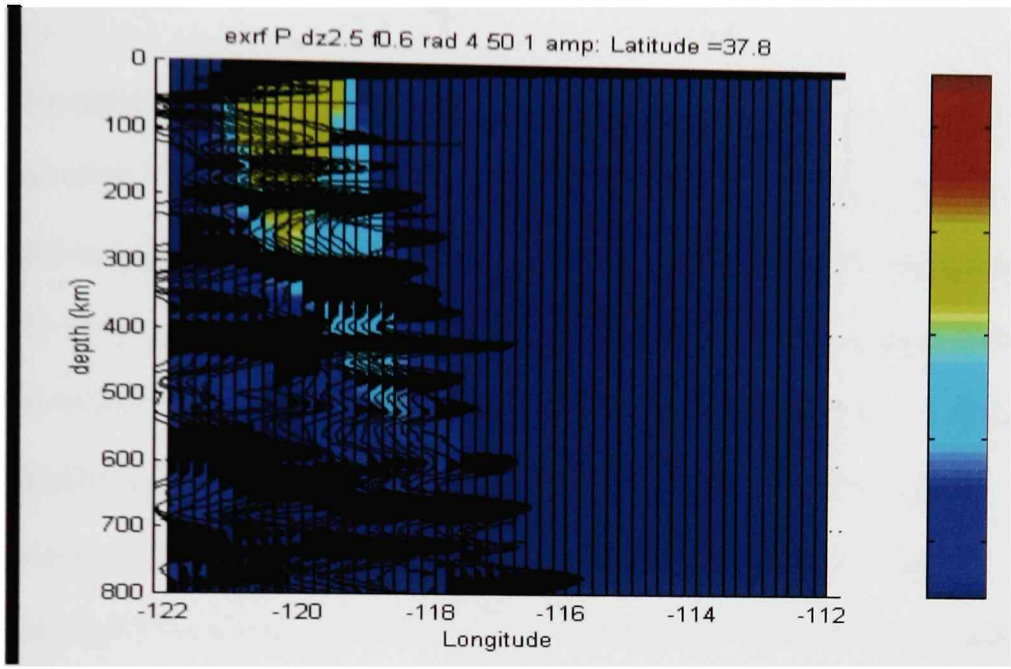

(a)

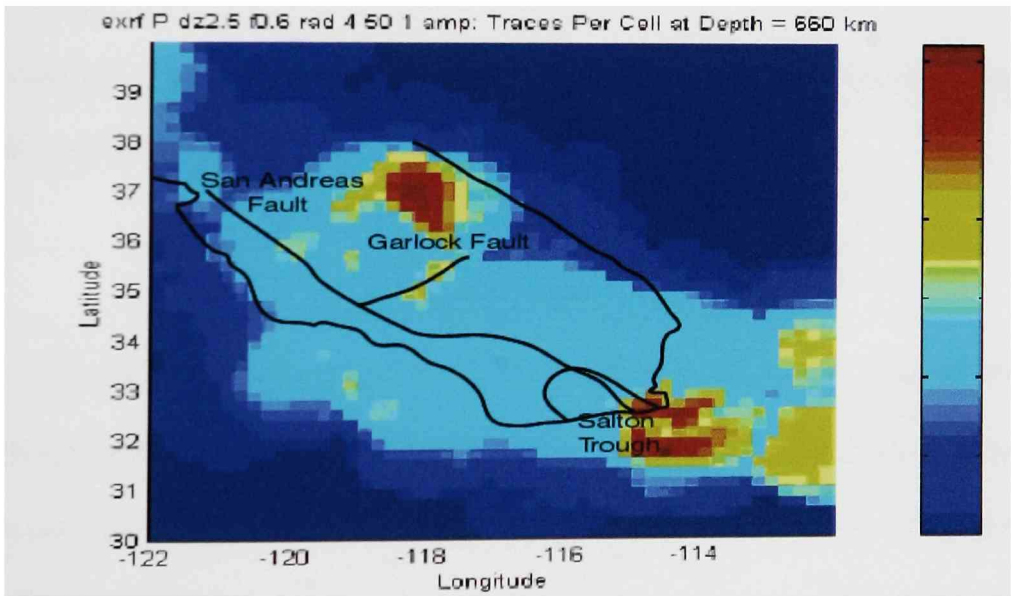

(b)

Figure 2.5. Figures depicting the number of traces found in each bin. (a) is a horizon located at 37.8° latitude. (b) is a horizontal view located 660 km depth. The color represents the number of traces contained in each bin.

CHAPTER III

DISCOPNTINUITIES THROUGHOUT THE MANTLE TRANSITION ZONE

The upper mantle transition zone is thought to be made up almost exclusively of phases of olivine and to a lesser degree garnet. Past studies have found discontinuities throughout the mantle transition zone at 410 km (olivine to spinel) and 660 km (spinel to magnesiowüstite and perovskite) depth (Simmons and Gurrola, 2000). Another boundary is thought to exist near the 520 km depth due to (β) Spinel transforming into (γ) Spinel as well as a garnet changing to an ilmenite phase at the 720 km discontinuity. The Clapeyron slopes of these horizons (discussed in chapter 2) will determine the topographic relief expected to be associated with temperature variations (Simmons and Gurrola, 2000). This thesis reproduces the work of Simmons and Gurrola (2000) with a greater quantity of data at a more even distribution providing a higher resolution image and improved interpretation.

3.1 Viewing Receiver Function Stacks

A 3D cube containing common conversion point stacked receiver functions was produced between 31° to 39° north Latitude and -114° to -122° west Longitude. Once horizons are found they are contoured throughout the study area. Figure 3.1 shows the 410 km discontinuity marked across all longitudes at 34.2° latitude. Receiver functions are seen to extend vertically in depth every 0.2° longitudes. The bottom figure in Figure 3.1 is depicting the same data as above with the amplitude of the receiver functions

spikes in color according to magnitude. Positive amplitudes are in red. Negative amplitudes are in blue and amplitudes near zero are in green. Mapping the 660 km discontinuity was done the same way and stood out clearly so it was easily found through out the entire cube (Figure 3.2). When all horizons have been traced a topographic map can be produced (Figure 3.3 and 3.4). The change in horizon elevation is seen as a variation in color across the cube (red is deep, blue is shallow). The 520 and 700 km discontinuities were found intermittently across the cube as previously reported by Simmons and Gurrola (2000).

Figure (3.1) is an east-west cross section at 34.2° latitude shown as A-A' on Figure (3.3). The 410 km discontinuity shows two depressions of ~ 20 km and 10 km in depth. The 20 km depression is centered at –117° West latitude labeled (20) and the 10 km depression is centered at –113.4° west latitude labeled (10) on Figure 3.1. The exothermic nature of the (α) olivine to (β) spinel phase change, hypothesized to control the 410, indicates that such positive variation in relative depth are due to a localized high temperature anomaly. A temperature change of 13°C per kilometer change is consistent with the clapeyron slope for the (α) olivine to (β) spinel phase change (Gurrola, 1995). This is determined by multiplying the density of rock by the gravity, which gives an estimate of change in pressure as a function of depth. This converts the Clapeyron slope from temperature and pressure to temperature and depth. Then multiplying the depth by the Clapeyron slope gives change in temperature of 13°C per kilometer. A temperature change of 260°C and 130°C would, therefore correlate with 20 km and 10 km depth anomalies respectively. Figure (3.2) depicts an east-west cross section, labeled B-B' on

Figure 3.4, with a small depression (10 km) located at 118.6° west latitude labeled (10). This topography is indicative of a cold spot (approximately 130°C) since the (β) Spinel to (γ) Spinel phase change is endothermic. The equal elevation changes in the 410km and 660km discontinuities are due to equal but opposite temperature changes, 130°C and -130°C, and is what is expected from their Clapeyron slope measurements. In Figure 3.5 two horizons appear to merge into each other. The spinel phase change is seen on top, approximately 660km, labeled (SP) while the garnet transition is mapped below, approximately 720, labeled (GR).

3.2 Interpretation of Horizons

410 and 660 km horizons were picked across the entire cube (Figure 3.1 and Figure 3.2, respectively). In all frequencies studied (frequencies = 0.2, 0.3, 0.4, 0.5 Hz) the 410 km and 660 km discontinuities were found and topographic maps throughout the entire study area were computed (Figure 3.3 and Figure 3.4, respectively). Lower frequencies or higher wavelengths are quieter and have better continuity because they won't pick up small crustal structures. Frequencies are increased in order to increase resolution but by increasing high frequency content noise levels are also increased. Once horizons are mapped at all frequencies the position of the horizons are compared to produce a horizon map that is consistent with the phases observed in all frequency images.

3.2.1 Multiple 660 km Discontinuities

Recent work by Simmons and Gurrola (2000) found multiple horizons at about 660 and 700 km that were interpreted as phase changes in the olivine and garnet mineral systems. These phase transforms may be due to subducted materials likely to accumulate where garnet changes to a less dense ilmenite phase and becomes more buoyant resisting further sinking. Simmons and Gurrola (2000) were able to detect the second ilmenite phase at all frequencies studied, but were only able to be maped continuously throughout the area at the lowest studied frequency of 0.2 cycles/second (Figure 3.5). This horizon is only visible across the entire section at low frequencies where signal generated noise due to crustal scattering is eliminated. This low noise level creates a cleaner looking receiver function. This is why more receiver functions are kept at the lower frequencies producing a more regionally continuous image.

3.2.2 520 km Discontinuity

The (β) spinel to (γ) spinel transform hypothesized to be found at a depth of 520 was only mappable at the lowest frequency of 0.2 cycles/second (Figure 3.6). The Clapeyron slope for the (β) spinel to (γ) spinel phase change hypothesized to be responsible for the 520 km discontinuity is exothermic, similar to the 410 km discontinuity and is 3 times steeper than that of the 410 km (Figure 1.2). The hypothesized 520 km deep phase change takes place over a large gradient from all (β) spinel to all (γ) spinel with mixing of these phases over the large gradational boundary.

The garnet mineral system may also play an important role in the transition zone (Gasparik, 1997). If so the zone of mixing would be diminished and become much sharper. Given the amplitude of short wavelength topography on the 410 km discontinuity it is reasonable to assume that, if present, the 520 km discontinuity may have enough topography to diminish the quality of the stacked image. It would disappear on the layer in locations with large bins or that is data rich. Ninety km of topography was found on the 520 compared to only 35 km on the 410 and 45 km on the 660 (Figure 3.7). This is nearly triple the relief of the 410 km which is expected given the increased gradient of the Clapeyron slope of the hypothesized 520 km discontinuity.

3.3 Mantle Thermometry

Many past seismic investigations have found velocity discontinuities that exist near the 660 km and 410 km depths. These discontinuities can be explained by phase changes of common minerals found in the mantle. The Clapeyron slopes of these phase changes can be applied to observed depth variation in the respective discontinuity to infer the temperature within the mantle. As discussed in chapter 1 if a phase change is exothermic then it will shallow in cool areas and deepen in hotter areas. Alternatively an endothermic phase change will tend to shallow in hot areas and deepen in cooler areas. By subtracting the depths of the 410 km discontinuity from the depths of the 660 km discontinuity, we produce an isopach map showing variations in transition zone thickness. The low frequency profiles tend to be less noisy and provide better continuity but they will have lower resolution. The higher frequency profiles would thereby provide

greater resolution but tend to be noisier. As a result all horizons were picked and then repicked projecting them on the seismic profiles from all frequencies until the horizon appear to be a best match to the signal at all frequencies. Isopach maps of this average topographic map of the 660 minus that of the 410 were used to create a map depicting the change in transition zone thickness (Fig 3.8).

3.3.1 Discussion of Temperature Distribution in the Mantle Transition Zone

Upper mantle temperature directly affects topography on the 410 and 660 km discontinuities discussed previously. Past experiments have determined that the temperature gradient in the mantle transition zone is approximately 13 °C for every kilometer of change (e.g. Gurrola 1995). Clapeyron slopes of the 660 and 410 are opposite in sign but are of nearly equal magnitudes in their gradients (Figure 3.3, 3.4). The temperature variation of the 520 would be similar to that of the 410 and 660 if the thermal anomalies are continuous through the transition zone. The temperature variations on the 520 km discontinuity are ~600 degrees (Figure 3.7). This is slightly larger than expected and may be explained by localized convection in the transition zone causing the hot areas to rise and cool areas to sink. Temperature ranges for all horizons fall within 50°C of each other implying that the temperature ranges of the anomalies don't vary as you progress upward in the mantle transition zone. This requires no alternate mechanics to explain localized heat sources. The positions of the anomalies change as you progress through the mantle and seem to make no discernable pattern. There are a few areas

where low temperature anomalies extend through the transition zone that may be due to crustal features, which will be discussed further in the next section.

A temperature map was created based on the differences in depths between the 410 and 660 km discontinuities (Figure 3.8). The depths of the 410 were subtracted from the depths of the 660 to produce a map of transition zone thickness (TZT). Changes in TZT were determined and thick TZT correlates to cold mantle while thinning in the TZT represents hot mantle. Hot areas are depicted in red and cool areas are in blue. These thermal anomalies can be compared to anomalies at shallower depths inferred from velocity tomography studies to identify possible links between lithospheric tectonics and the transition zone. The strongest correlation between lithospheric features and transition zone temperature appear in the mantle beneath the Transverse Ranges, southern California.

3.4 Discussion of Transition Zone Thickness

Variations in transition zone thickness (fig 3.8) can be used to infer variations in transition zone temperature. Thicker regions indicate a cool mantle and thinning of the transition zone indicates regions of higher mantle temperatures. A North-South trend of high temperature between -119° and -120° west longitude and 33° to 39° north latitude lies directly under the California's Great Central Valley (GCV). Another high temperature anomaly lies from 34° to the edge of the study area at 37° latitude and -116° to -117° longitude beneath the Mojave Desert labeled (MD) and Death Valley which is North of the propagating east Pacific rise in the Gulf of California. It is possible that the

Salton Trough is the northern extension of the Gulf of California but some researchers say it is a pull apart basin (Elders, 1972). A thick transition zone exists beneath the Salton Trough, extending south to the Gulf of California, which indicates a low temp anomaly beneath this area. This would indicate that the heat source for the spreading ridge in the Gulf of California does not extend to the 410 km depth directly beneath southern California. Tomographic studies infer high heat in the Salton Trough to a depth of 290 km (Figure 3.9) (Humphreys and Clayton, 1990), which is consistent with the presence of a pull apart basin. Some researchers have suggested that the shallow heat anomaly associated with the Salton Trough is the result of pressure release melting, because it is a pull apart basin (Larson et al., 1968; Moore and Buffington, 1968; Elders et al., 1972). However, the thermal anomaly in the transition zone to the north of this feature, beneath Death Valley, may indicate a northward propagation of the heat source related to the northern propagation of the ridge that is opening the Gulf of California. Owens et al. (2000) found that the lithospheric thermal anomaly associated with lithospheric rifting on either side of the Tanzanian craton was fed by a single anomaly in the transition zone at the South end of the Eastern rift. This is precedent for a similar mechanism to be related to the Gulf of California, that is that the thermal anomaly in the transition zone may have migrated north but may still feed the upper lithosphere beneath the spreading ridge. Although this does explain the features seen it is not any more probable than the hypothesis that the Salton Trough is a pull apart basin. In fact tomography models of southern California mantle do not show a link between deeper thermal anomalies and the thermal anomaly beneath the Salton Trough.

A smaller low temperature anomaly (indicated by the thicker transition zone) located at 118° west Longitude and between 34° and 35° north latitude labeled (D1) lies directly beneath a high velocity anomaly inferred from a tomographic study (Figure 3.9) (Humphreys and Clayton, 1990). The tomographic study used seismic velocities to determine velocity changes in the subsurface. High velocities represent cool areas and low velocities represent hot areas. The low velocity anomaly was found to extend to at least 300 km depth. Humphreys and Clayton, 1990 interpret this temperature anomaly to be a subcrustal lithospheric "drip" (Figure 3.10) beneath the Transverse Ranges. In Figure 3.10 the cartoon to the left represents subduction at equal rates from both north and south. The picture to the left represents one-sided subduction only from the south. Second from the left is a picture of two-sided subduction at different rates without coupling between sides. The last picture is of two-sided subduction at different rates with coupling between the sides. This "drip" feature is essentially a localized, micro subduction event. The resolution of the data does not give enough information to differentiate which subduction diagram is correct. The lithosphere would have a lower temperature anomaly as it sinks or "drips" as that observed in a subducting slab. With a lithospheric thickness of 40 to 70 km (Humphreys, Hager 1990) the drip should be resolvable given the frequency content of the stacked images. The Fresnel Zones for the frequency range of each seismic image is tabulated in Table (3.1).

Humphreys and Hager's model only places the drip to a depth of about ~ 300 km, but suggests that stretching of one third of the length is possible. A gravity study

done across the Transverse Ranges (Sheffels and McNutt, 1986) found a gravity low that is best explained by one-sided lithospheric subduction (Fig 3.11). Contractional tectonics have been acting on the Transverse Ranges for the past 10 My (Huffman, 1972; Dickenson et al 1972; Meisling and Weldon, 1989). Over that time approximately 240 km of San Andreas strike slip fault system slip has occurred (Huffman, 1972; Dickenson et al 1972; Meisling and Weldon, 1989). It is unclear as to whether the descending body has remained in one piece or has been fragmented into pieces under its own weight as it descends. If the body of the slab is one sided and it is still in one piece then its maximum length of the drip should be equal to the amount of slip on the San Andreas Fault in that area. The depth extent of the "drip" can be approximated by adding the 240 km of San Andreas slip to the depth of the base of the lithosphere ~ 90 km which results in the 330 km depth mentioned above. The 240 km of lithospheric "drip" could then be stretched by one third under its own weight (Humphreys and Hager, 1990) producing a 320 km "drip" under the 90 km base of the lithosphere, which would result in a 410 km deep anomaly. Although the 410 km depth only places the base of the "drip" near the (α) olivine to (β) Spinel phase change, this phase boundary will be higher due to the cool temperature of the drip. This temperature change could raise the depth of the contact to ~380 km depth. As the drip passed through the (α) olivine to (β) Spinel phase contact it could become more dense and begin to stretch.

Humphreys and Hager (1990) did imply that the crustal kinematics differ from the corresponding subcrustal lithosphere. This implies the existence of decoupling zone between the crust and lithosphere by which more lithosphere could have been subducted

compared to movement on the San Andreas Fault system. If the lithosphere began moving prior to fault slip or faster than the crust moves then the "drip" could extend further than the 410 km depth. This excess movement of the lithosphere below the crust would be necessary to explain excess depth needed for the "drip" to reach the 660 km depth. An alternate model to extend this anomaly to the 660 is that the drip may become detached over time as a result of increased pull due to the density change at the 410 km depth. The increase in pull will cause the slab to break and a chunk will sink to the 660 discontinuity where it will become more buoyant due to the endothermic nature of the 660. This may have brought the "drip" to rest at the 660 km discontinuity creating a cool spot. This anomalous cool spot would explain the thickening of the transition zone in this region.

If decoupling is occurring and the lithosphere is stretching vertically under its own weight this could explain the heating of the lithosphere under the Salton Trough. Even if the lithosphere is not detached you could get more than a 240 km drip since the Salton Trough is a pull apart basin. The fault could be moving more than 240 km and be compensated by the pull apart. Tomographic work suggests a high temperature anomaly beneath the Salton Trough between 60 and 100 km depth. This depth matches the depth of the lithosphere in that region. A receiver function study of the crust mantle boundary done across the Peninsular Ranges done by Lewis et al (2000) found the Moho thins from west to east (Figure 3.12). This thinning would correspond to lithospheric extension under the Salton Trough as the "drip" to the North subducts under its own weight. The lithospheric extension would cause pressure release resulting in melting which releases

heat. An alternate explanation for the increased heat is that the lithosphere beneath this region may be detached and moving faster than the surface fault. As a result the lithosphere may be stripped from beneath the Salton Trough allowing the hotter asthenophere to rise to replace the missing lithosphere resulting in hotter material at shallower depths (Figure 3.12).

It should be noted that another "drip" proposed by Saleeby et. al (2003) is found at -118° west longitude and between 35° and 35.5° north latitude (D2) beneath the southern edge of the Sierra Nevadas. Saleeby suggests a different mechanism for this drip than that proposed by Humphries for the Transverse Ranges drip and Saleeby does not propose that their "drip feature" feature would extend to the transition zone. But the drip feature proposed by Saleeby is believed to extend to at least 200 km and there is strong correlation between it and a low temperature anomaly in the Transition zone observed in this study. The Death Valley (DV) pull apart basin could be created by the Garlock strike-slip fault causing this Drip. Alternatively if the drip originated first the Garlock fault could propagate faster speeding the motion on the Death Valley basin. These same mechanisms could be used to explain this drip as the one under the Transverse Ranges.

3.5 Conclusions

The 440 km and 660 km discontinuities found in previous studies were reproduced throughout the entire study area at all frequencies used. A deeper discontinuity (720 km discontinuity) thought to be the result of an ilmenite to perovskite

phase transform was identified in profiles at many frequencies. However, it was only traceable across the entire region in the profile produced from the lowest frequency data (0.2 Hz). This could be the result of noise reduction and removal of crustal scattering in the lower frequency image. Evidence for a 520 km discontinuity was identified in many of the profiles. But in many regions this discontinuity may be too gradational or too structured to be resolvable under current data resolution. These results merely verify observations made from earlier work (Simmons and Gurrola, 2000; Simmons, 2000) done with about half the data available at this time. These earlier studies were not able to produce images sufficient to resolve the small-scale features discussed above.

Variation in transition zone thickness indicates at the very least geographic correlations between crustal anomalies and temperature anomalies extend into the transition zone. There appears to be a strong correlation between a low temperature anomaly inferred to be within the transition zone and a lithospheric "drip" believed to be related to the localized compressional event responsible for the transverse ranges. This would mean that the drip reaches depths much deeper than previously thought, possibly as deep as 660 km. A low temperature anomaly was however found to exist within the transition zone beneath the Salton Trough. The area of high heat below the Salton Trough and Northern Gulf of California is thought to come from a lithospheric source or possibly from rising asthenophere. This is also consistent with heating that would be associated with lithospheric stretching. As the lithosphere thins the asthenophere would rise to compensate and bring hotter material towards the surface. This stretching may be necessary for the drip feature inferred beneath the transverse ranges to extend into the

transition zone.

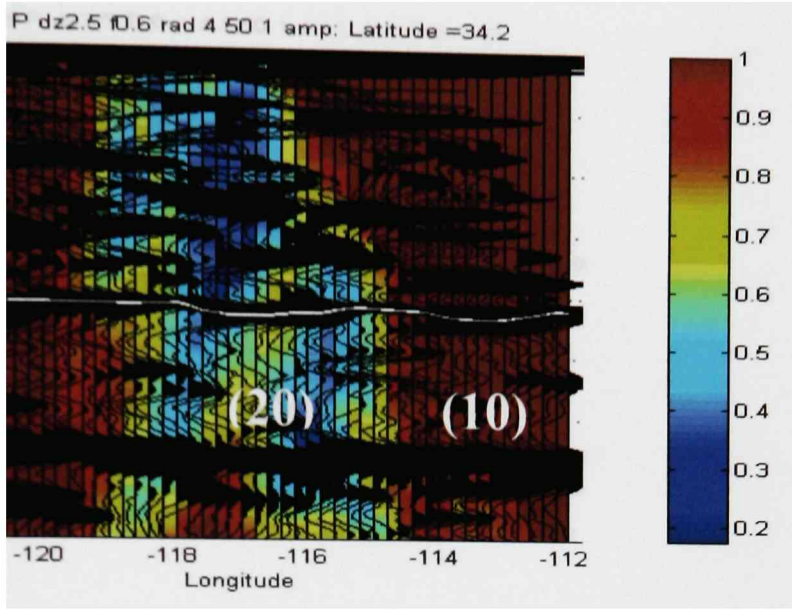

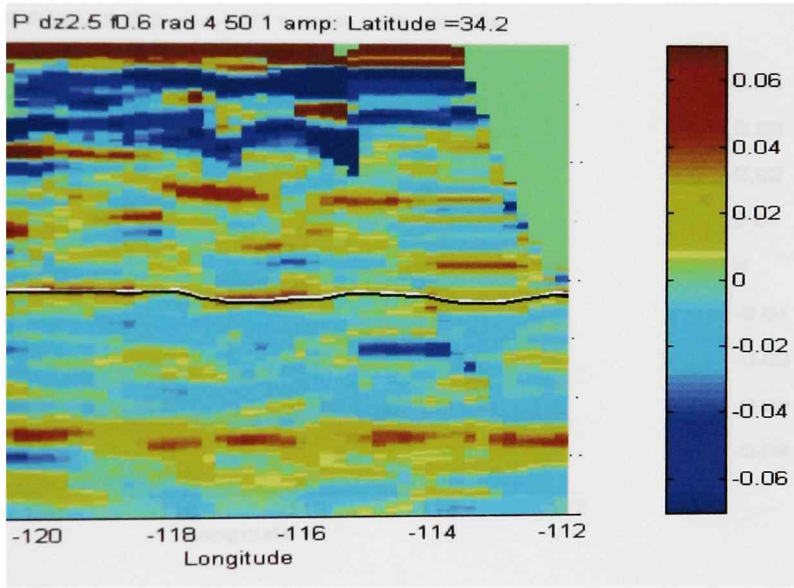

slice through 34.2°latitude depicting 410 km horizon.
:k (b). (a) shows P-to-S converted waves with background colors
ius of the bin necessary include the requisite minimum number of
:tacked into a bin. It is, therefore, indicative of resolution of the
ation. (b) shows amplitudes of waves, positive in red and negative in

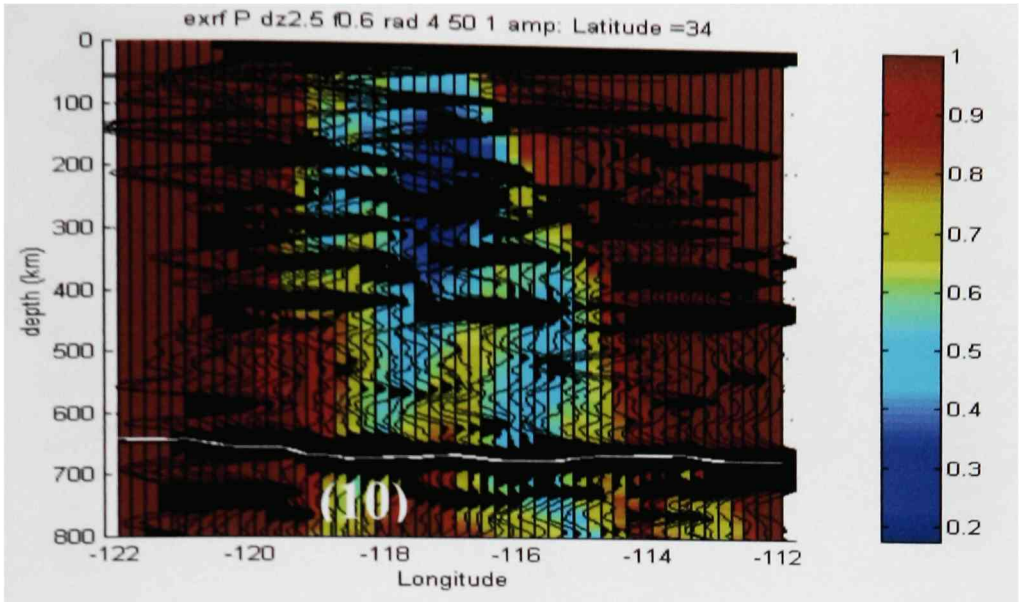

(a)

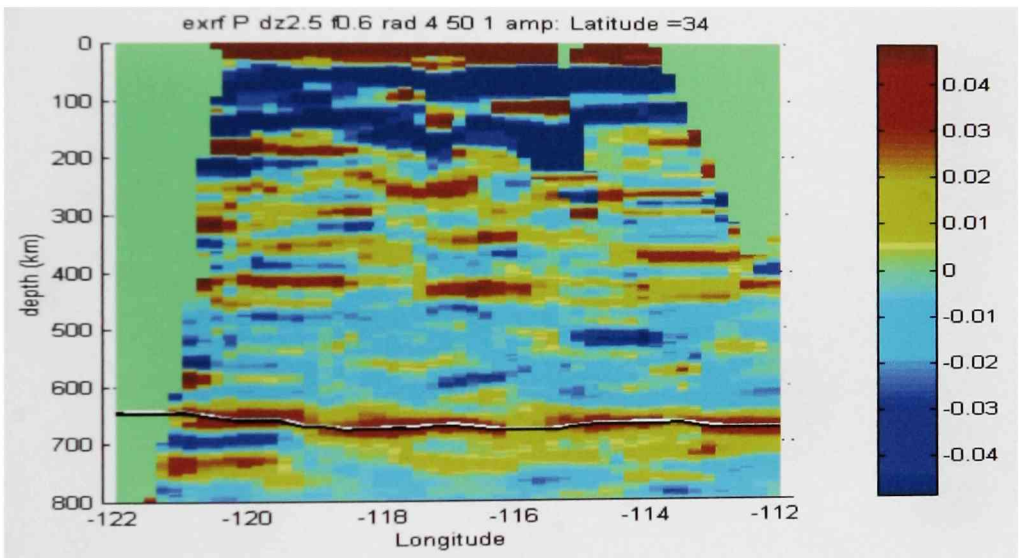

(b)

Figure 3.2. Vertical slice through 34° latitude depicting 660 km horizon.
In white (a) and black (b). (a) shows P-to-S converted waves with background colors representing the radius of the bin necessary include the requisite minimum number of stations and events stacked into a bin. It is, therefore, indicative of resolution of the image at a given location. (b) shows amplitudes of waves, positive in red and negative in blue.

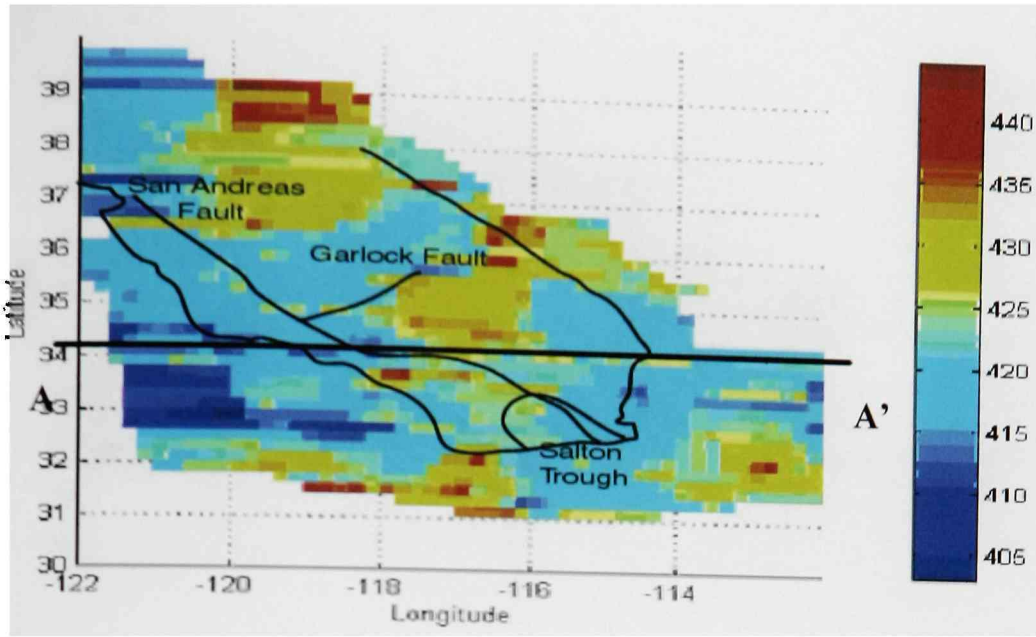

(a)

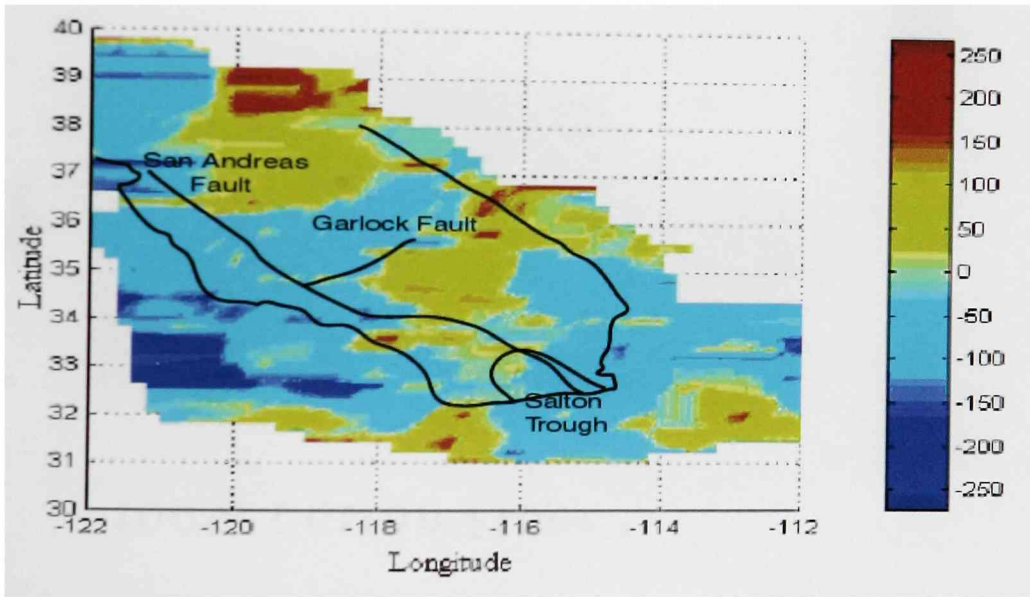

(b)

Figure 3.3. Maps of 410 km horizon.
(a) is a topographic map of 410 km discontinuity across 3D cube of research area. Colors represent depths to discontinuity in kilometers below sea level. (b) shows temperatures across horizons. Color bar represents change on thermometry in °C. A to A' represents the area of the cross section in Figure 3.1.

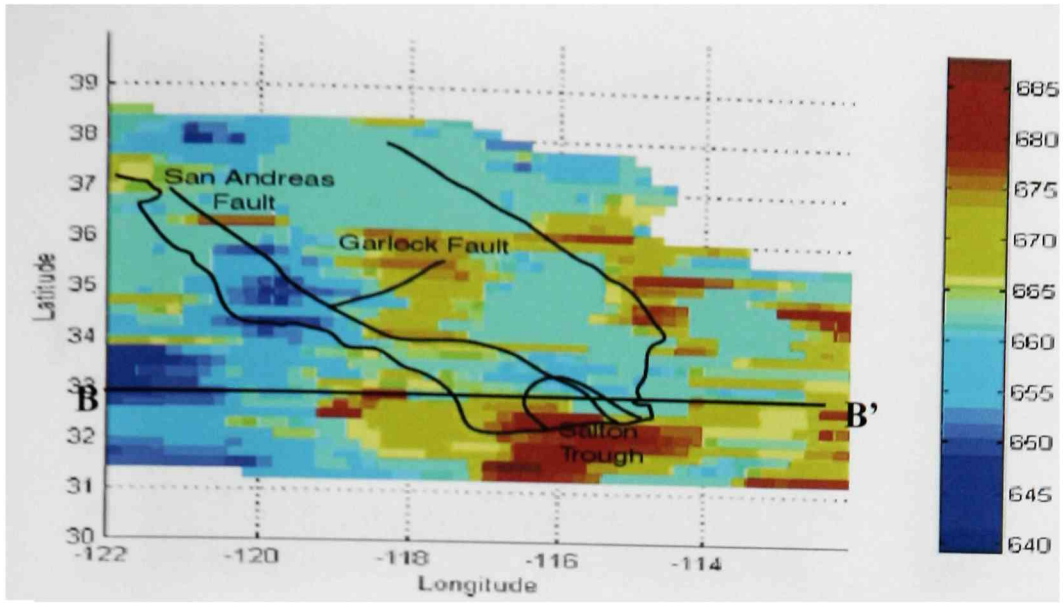

(a)

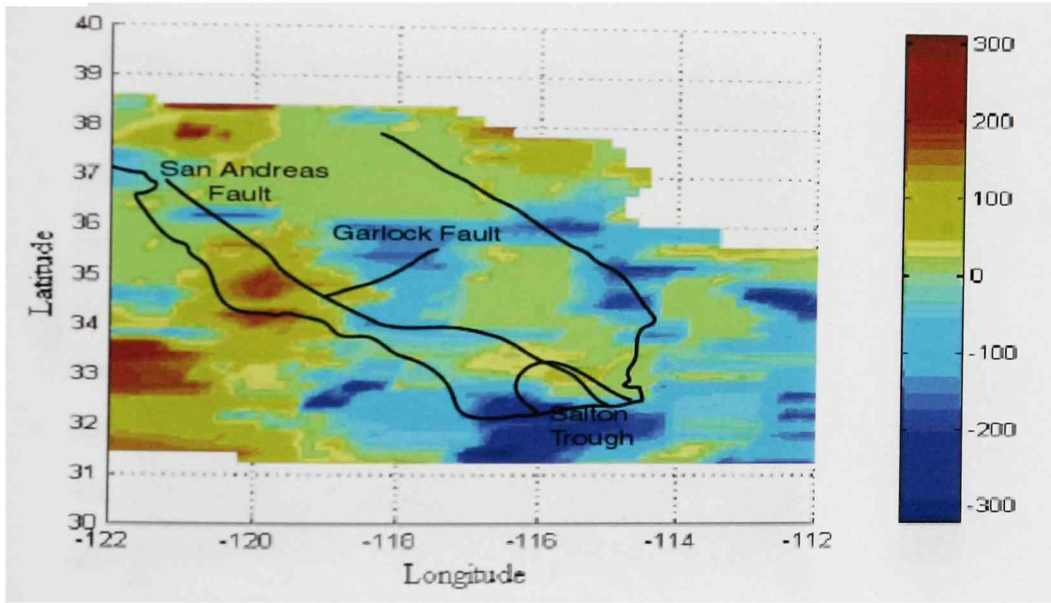

(b)

Figure 3.4. Maps of 660 km horizon.
(a) is an topographic map of 660 km discontinuity across 3D cube of research area. Colors represent depths to discontinuity in kilometers below sea level. (b) shows temperatures across horizons. Color bar represents change on thermometry in °C. B to B' represents the area of the cross section in Figure 3.2.

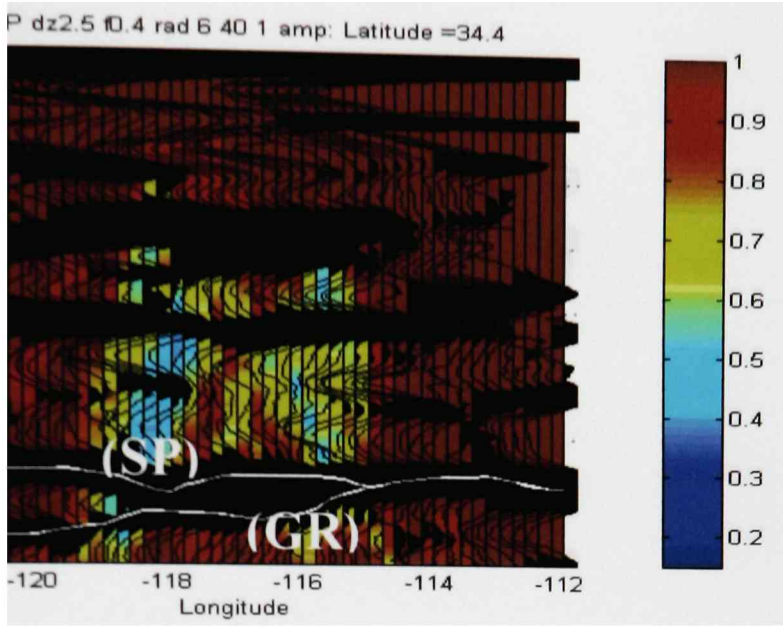

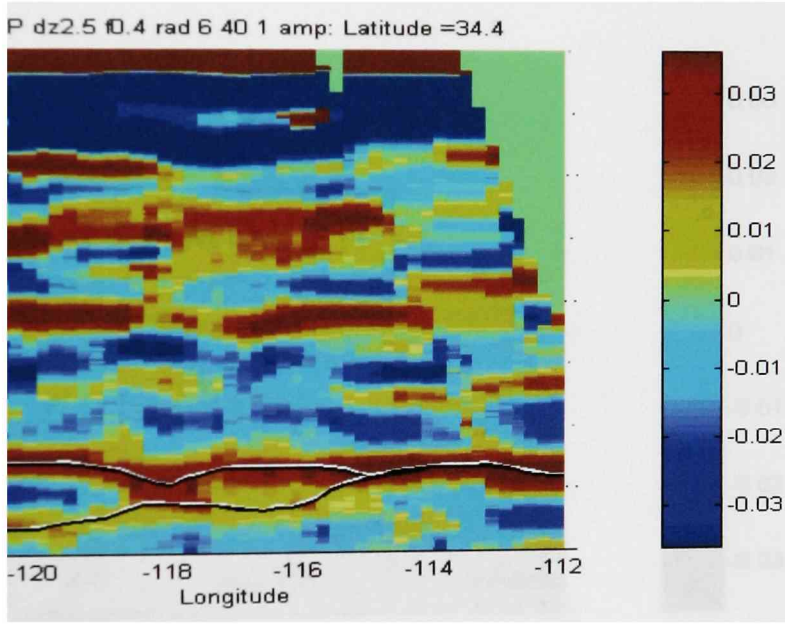

slice through 34.4° latitude.
phase changes present at the 660 km horizon in white (top figure) and
). (a) shows P-to-S converted waves with background colors
us of the bin necessary include the requisite minimum number of
tacked into a bin. It is, therefore, indicative of resolution of the image
b) shows amplitudes of waves, positive in red and negative in blue.

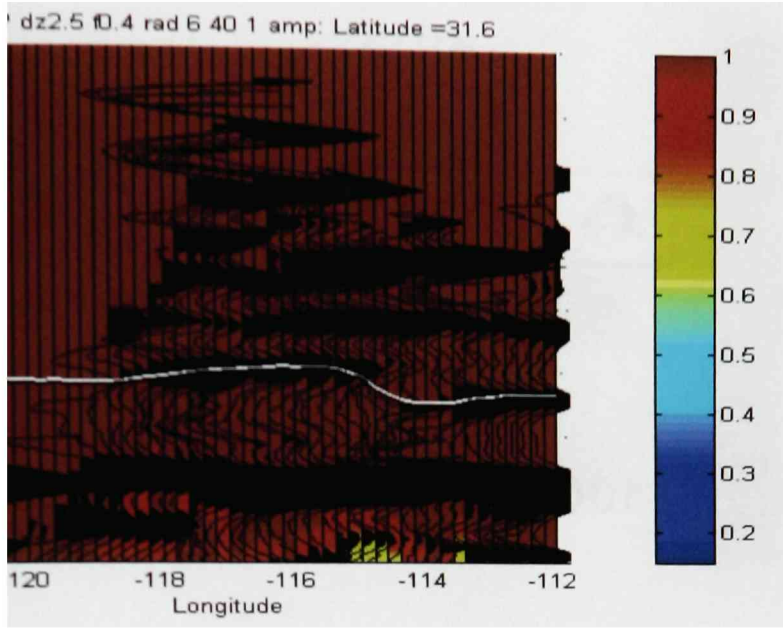

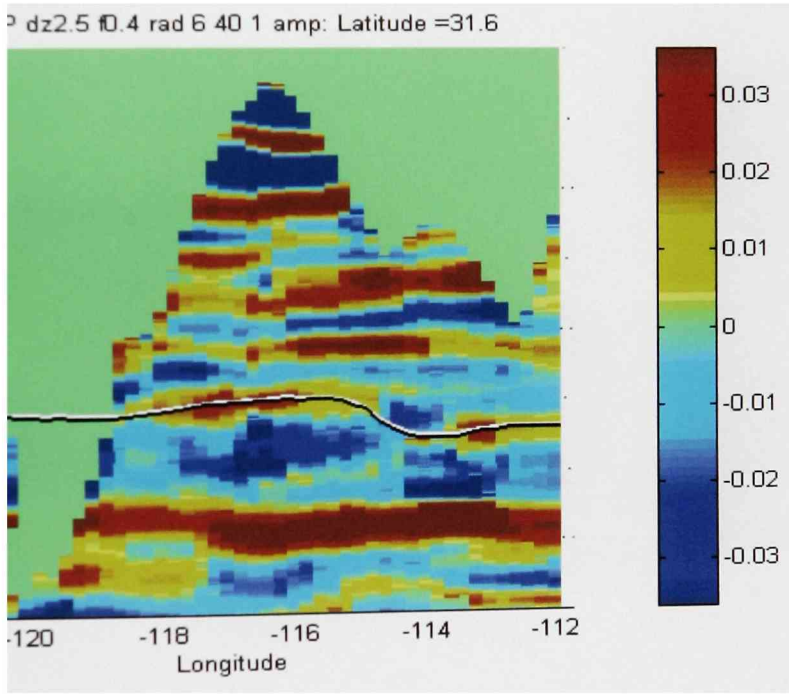

slice through 31.6° latitude.
ɪm horizon in white (top figure) and black (bottom figure). (a)
ted waves with background colors representing the radius of the bin
ɛ requisite minimum number of stations and events stacked into a
indicative of resolution of the image at a given location. (b) shows
, positive in red and negative in blue.

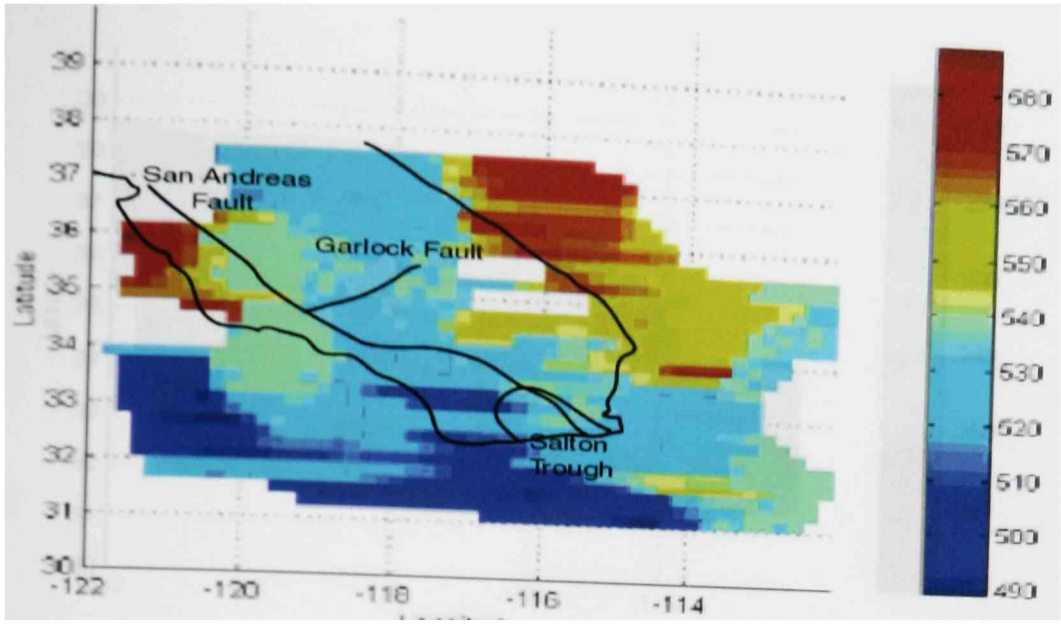

(a)

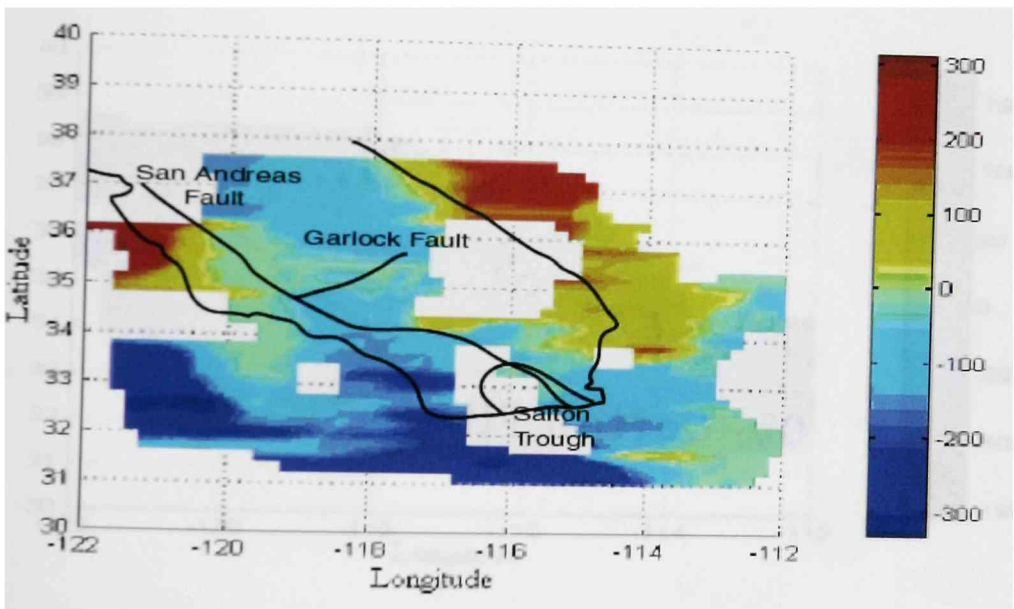

(b)

Figure 3.7. Maps of 520 km horizon.
(a) is an isopach of 520 km discontinuity across 3D cube of research area. Colors represent depths to discontinuity in kilometers below sea level. (b) shows temperatures across horizons. Color bar represents change on thermometry in °C.

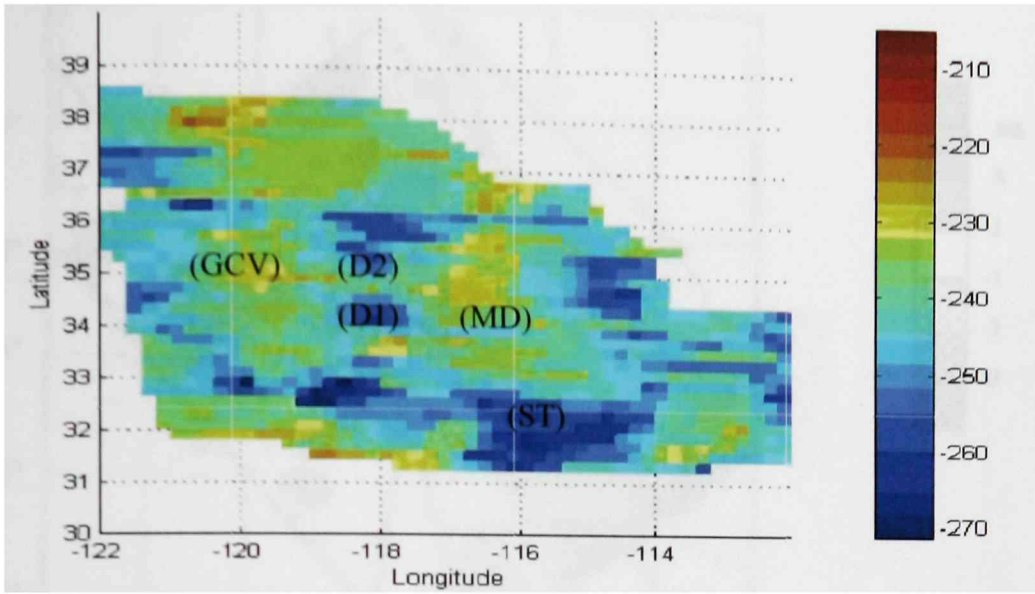

(a)

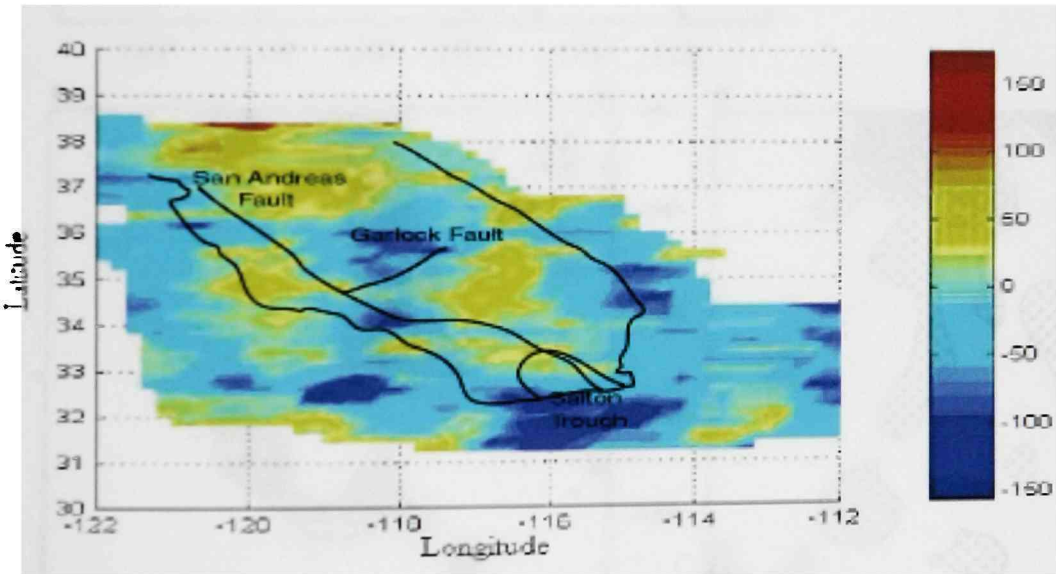

(b)

Figure 3.8. Isopach of differences between the 440 km and 660 km discontinuity. (a) is in depth where colors represent depths in kilometers between discontinuities. (b) shown temperatures in the mantle transition zone in °C.

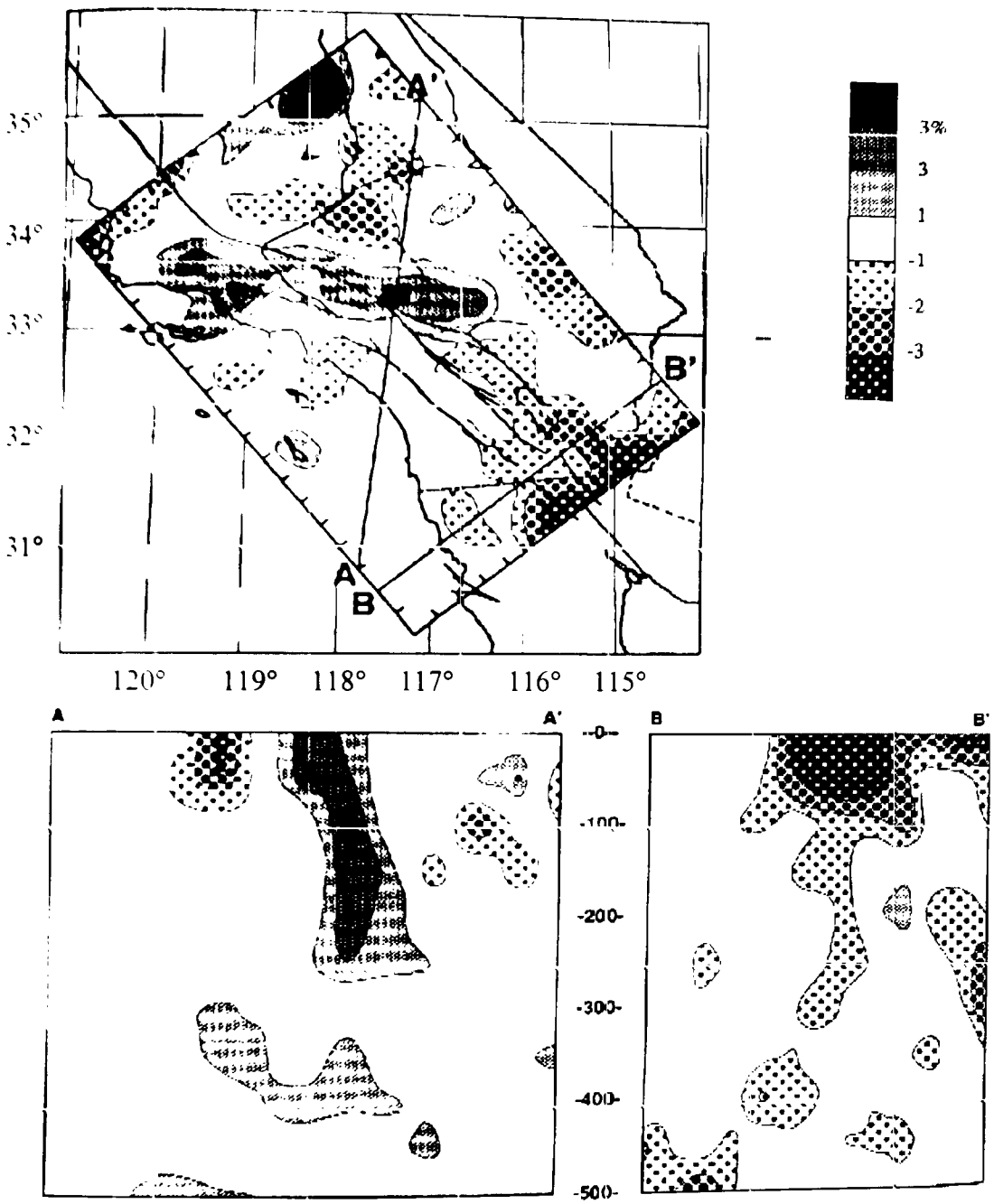

Figure 3.9. Tomographic image of the upper-mantle seismic structure beneath southern California.

The major anomalies seen are the volume of high-velocity mantle beneath the Transverse Ranges and the region of slow mantle beneath the Salton Trough.

Source: Humphreys and Clayton (1990)

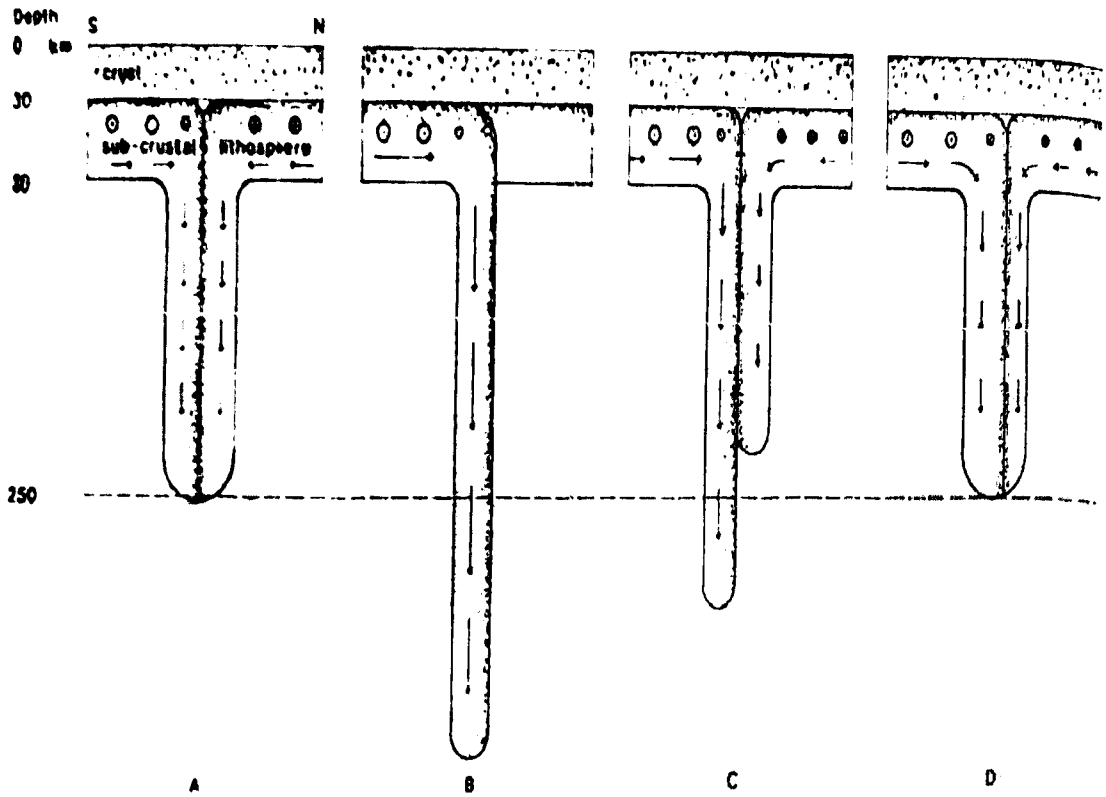

Figure 3.10. Schematic diagrams illustrating possible means by which subcrustal lithosphere may be consumed.
Circled dots indicate a component of motion towards the viewer, and circled pluses indicate motion away. Crustal motions are not shown in the figure. (a.) Asymmetrical situation in which both sides converge and sink at the same rate. (b.) Single-sided sinking. (c.) and (d.) two possible means of asymmetrical, two-sided convergence and sinking.
Source: Humphreys and Hager (1990)

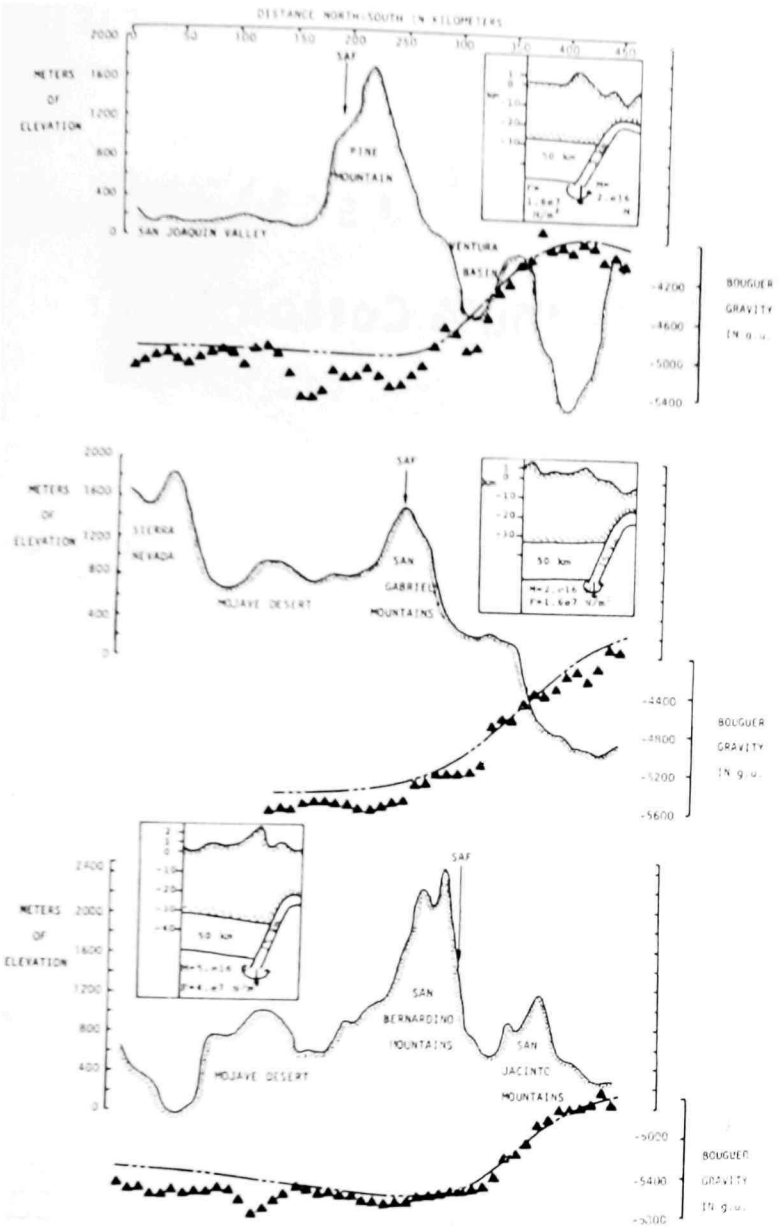

Figure 3.11. Gravity/topography profiles through the Transverse Ranges. Solid triangles represent Bouguer gravity referenced to 4 km below the surface. Patterned lines plot theoretical gravity from Airy compensation assuming a crustal thickness of 25 km at sea level. Small insets showing the crustal model used in the gravity calculation are drawn to scale, with 40:1 vertical exaggeration for the topography and 8:1 vertical exaggeration for the Moho.
Source: Sheffels and McNutt (1986)

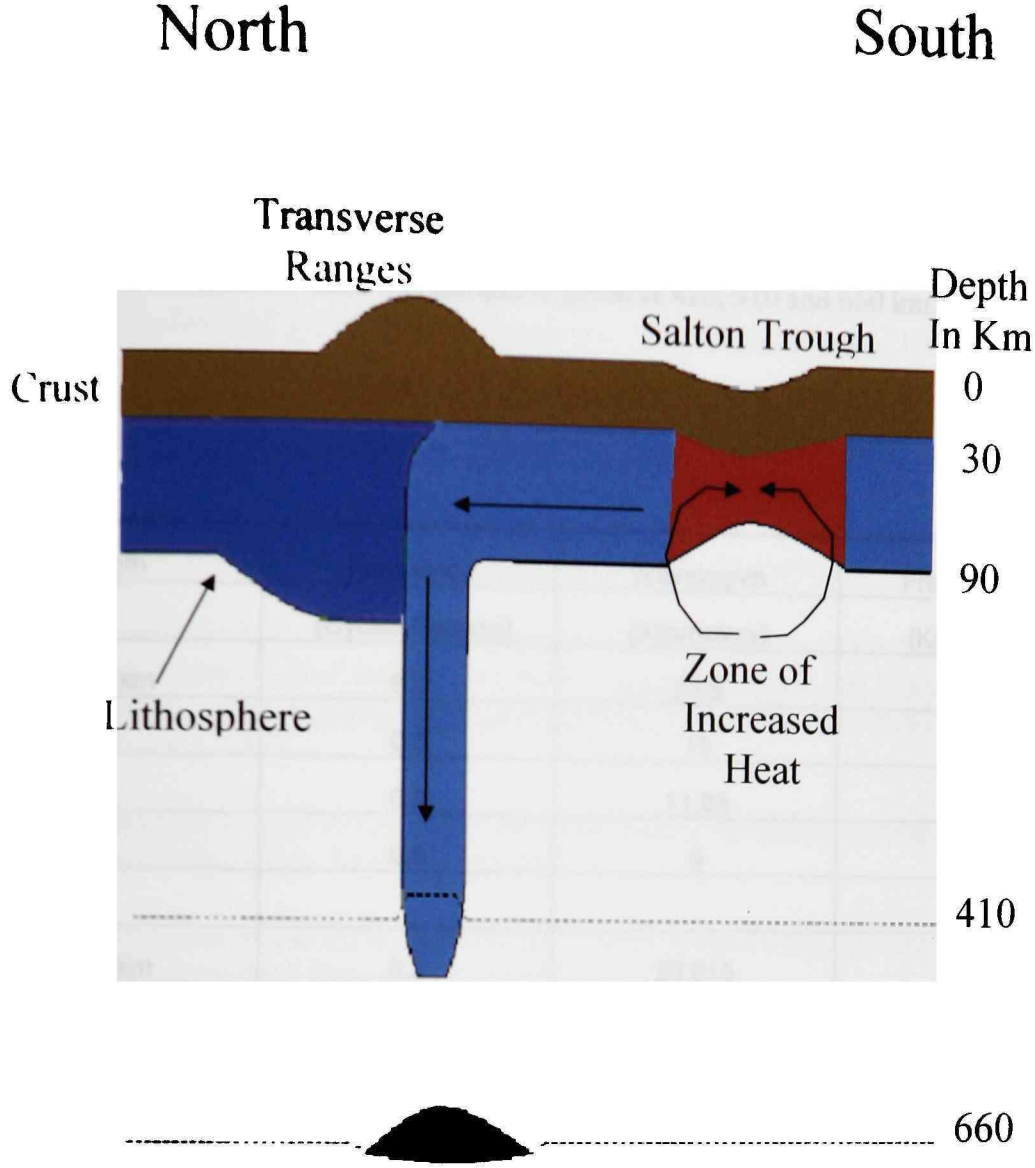

Figure 3.12. Depiction of interaction between "Drip" and thinning below Salton Trough.

As the drip sinks the Transverse Ranges rise and the lithosphere beneath the Salton Trough thins due to stretching. Hot mantle rises beneath the Salton Trough to compensate for the extra space.

Table 3.1. Table containing Frequencies and their corresponding wavelengths. The Fresnel zones for each wavelength is given at 420, 510 and 660 km depth.

Depth	Frequency (Cycles/Second)	Wavelegnth (Kilometers)	Fresnel Zone (Kilometers)
410 km	0.2	22.5	67.92
	0.3	15	55.45
	0.4	11.25	48
	0.5	9	42.95
520 km	0.2	23.215	76.94
	0.3	15.477	62.821
	0.4	11.608	54.405
	0.5	9.286	48.66
660 km	0.2	24.123	89.222
	0.3	16.082	72.85
	0.4	12.062	63.09
	0.5	9.649	56.429

REFERENCES

Akaogi, M., Ito, E. and Navrosky, A. "Olivine-modified spinel-spinel transitions in the system Mg_2SiO_4-Fe_2SiO_4: calorimetric measurements, thermochemical calculation, and geophysical applications." J.Geophys. Res., 94 (1989), 15671-16685

Anderson, D.L. Theory of the Earth. Oxford: Blackwell Sci. Pub., 1989.

Atwater, T. "Implications of plate tectonics for the Cenozoic tectonic evolution of western North America." Geol. Soc. Amer. Bull., 81 (1970), 3515-3535.

Atwater, T. and Stock, J. "Pacific-North America Plate Tectonics of the Neogene Southwestern United States: An Update." Integrated Earth and Environmental Evolution of the Southwestern United States., Columbia, MD: Bellwether Publishing, 1998.

Bird, P. "Laramide crustal thickening event in the Rocky Mountains foreland and Great Plains." Tectonics, 3 (1984), 741-758.

Bird, P "Formation of the Rocky Mountains, western United States:A continuum computer model." Science, 239 (1988), 1501-1507.

Buland, R. and Chapman, C.H. "The computation of seismic travel times." Bull. Seism. Soc. Am., 73 (1983), 1271-1302.

Burdick, L.J. and Langston, C.A. "Modeling crustal structure through the use of converted phases in the teleseismic body waveforms." Bull. Seism. Soc. Amer., 67 (1997), 677-692.

Cheadle, M.J., et al. "The deep crustal structure of the Mojave Desert, California, from COCORP seismic reflection data." Tectonics, 5 (1986), 293-320.

Coney, P.J. "Plate tectonics and the Laramide orogeny, in Woodward, L.A., and Northrop, S.A." Tectonics and mineral resources of southwestern North America. New Mexico Geological Society Special Publication No. 6, 1976.

Cross, T.A. "Tectonic controls of foreland basin subsidence and Larimide-style deformation, western United States." Inter. Assoc. Sedimentol. Spec. Publ., 8 (1986), 15-39.

Davis, G.F. Dynamic Earth Plates, Plumes and Mantle Convection., UK: Cambridge, 1999.

Dickonson, W.R. "Relations of andesite, granites, and derived sandstones to arc-trench tectonics." Reviews in Geophysics and Space Physics, 8 (1970), 813-860.

Dickinson, W.R., Cowan, R.G., Schweickert, W.A. "Test of new global tectonics: Discussion." AAPG Bull., 56 (1972), 375-384.

Dickenson, W.R. and Snyder, W.S. "Plate tectonics of the Laramide orogeny." Geol. Soc. America Mem., 151 (1978), 355-366.

Dueker, K.G. and Sheehan, A.F. "Mantle discontinuity structure from midpoint stacks of converted P to S waves across the Yellowstone hotspot track." J. Geophys. Res., 102 (1997), 8313-8327.

Dueker, K.G. and Sheehan, A.F. "Mantle discontinuity structure beneath the Colorado Rocky Mountains and High Plains." J. Geophys. Res., 103 (1998), 7153-7199.

Duffy, T. and Anderson, D.L. "Seismic velocities in mantle minerals and the mineralogy of the upper mantle." J. Geophys. Res., 94 (1989), 1895-1912.

Dziewonski, A.M. and Anderson, D.L. "Preliminary reference earth model." Phys. Earth Planet. Inter., 25 (1981), 297-356.

Elders, W.A. et al. "Crustal spreading in southern California" Science, 178 (1972), 15-24.

Engebretson, D.A., Cox, A. and Gordon, R.C. "Relative motions between oceanic and continental plates in the Pacific Basin." Geol. Soc. Amer. Spec Pap., 206 (1985), 59.

Engebretson, D.A., Cox, A. and Thompson, G.A. "Correlation of plate motions with continental tectonics: Laramide to Basin-Range." Tectonics, 3 (1984), 115-119.

Gasparik, T. "A model for the layered upper mantle." Phys. Earth. Planet. Inter., 100 (1997), 197-212.

Gurrola, H. "Investigation of the Upper Mantle Transition Zone Through Velocity Spectrum Stacking of Receiver Functions" Ph. D. Dissertation, Scripps Institution of Oceanography, San Diego, California, 1995.

Huffman, O.F. "Lateral displacement of upper Miocene rocks and Neogene history of offset along the San Andreas fault in central California" Geol. Soc. Am. Bull., 83 (1972), 2913-2946.

Humphreys, E., Clayton R. "Topographic Image of the Southern California Mantle." J. Geoph. Res., 95 (1990), 19,725-19,746

Humphreys, E. Hager B. "A Kinematic Model for the Late Cenozoic Development of Southern California Crust and Upper Mantle." J. Geophy. Res., 95 (1990), 19,747-19,762.

Ingersoll, Raymond V. "Phanerozoic Tectonic Evolution of Central California and Environs." Integrated Earth and Environmental Evolution of the Southwestern United States., Columbia, MD: Bellwether Publishing, 1998

Ito, E. and Takahashi, E. "Postspinel transformations in the system $Mg_2SiO_4 - Fe_2SiO_4$ and some geophysical implications." J. Geophys. Res., 94 (1989), 10637-10646.

Jordan T.H. "Structure and formation of Continental Tectosphere" Journal of Petrology, (1988), 11-37

Kasura, T. and Ito, E. "The systems Mg_2SiO_4 Fe_2SiO_4 at high pressures and temperatures: Precise determination of stabilities of olivine, modified spinel and spinel." J. Geophys. Res., 94 (1989), 15663-15670.

Trubitsyn, V.P., Mooney, W.D., Abbott, D.H. "Cold cratonic roots and thermal blankets; how continents affect mantle convection." Geol. Soc Amer., The lithosphere of western North America and its geophysical characterization International Book Series, 7 (2003), 458-475.

King, S.D. "Introduction to the special section on the transition zone." J. Geophys. Res., 99 (1994), 15779-15782.

Kennett, B.L.N. and Engdahl, E.R. "Travel times for global earthquake location and phase identification" Geophys. J. Int., 105 (1991), 429-465.

Langston, C.A. "The effects of planar dipping structure on sources and receiver responses for constant ray parameters." Bull. Seism. Soc. Am., 67 (1977), 1029-1050.

Langston, C.A. "Structure under Mount Rainier, Washington, inferred from teleseismic body waves." J. Geophys. Res., 84 (1979), 4749-4762.

Langston, C.A. "Evidence for the subduction lithosphere under southern Vancouver Island and western Oregon from teleseismic P wave conversions." J. Geophys. Res., 86 (1981), 3857-3866.

Langston, C.A. "Scattering of teleseismic body waves under Pasadena, California." J. Geophys. Res., 94 (1989), 1935-1951.

Larson, R.L., Menard, H.W., Smith, S.M., "Gulf of California; A result of ocean-floor spreading and transform faulting." Science, 161 (1968), 781-784.

Lewis, J., Day, S., Magistrale, H., Eakins, J., Vernon, F. "Regional crustal thickness variations of the Peninsular Ranges, southern California" Geology, 28 (2000), 303-306.

Meisling, K.E., Weldon, R.J. "Late-Cenozoic tectonics of the northwestern San Bernardino Mountains, southern California" Geol. Soc. Am. Bull., 101 (1989), 106-128

Moore, D.G., Buffington, E.C. "Transform faulting and growth of the Gulf of California since the Late Pliocene." Science, 161, (1968), 1238-1241.

Moores, Eldridge M., Twiss, Robert J. Tectonics, New York: W.H.Freeman and Company, 1995.

Owens, T.J. "Determination of crustal and upper mantle structure from analysis of broadband teleseismic P-waveforms." Ph.D. Dissertation, University of Utah, Salt Lake City, Utah, 1984.

Owens, T.J. and Crosson, R.S. "Shallow structure effects on broadband teleseismic P waveforms." Bull. Seism. Soc. Am., 78 (1988), 96-108.

Owens, T.J. and Crosson, R.S. and Hendreckson, M.A. "Constraints on the subduction geometry beneath western Washington from broadband teleseismic waveform modeling." Bull. Seism. Soc. Am., 78 (1988), 1319-1334.

Owens, T.J., Nyblade, A.A, Gurrola, H., Langston, C.A. "Mantle Transition Zone Structure beneath Tanzania, East Africa" Geophy. Res. Letters, 27 (2000), 827-830

Owens, T.J., Taylor, S.R., Zandt, G., "Crustal structure at regional seismic test network stations determined from inversion of broadband teleseismic P waveforms." Bull. Seism. Soc. Am., 77 (1987), 631-662.

Owens, T.J., Zandt, G., Taylor, S.R. "Seismic evidence for an ancient rift beneath the Cumberland Plateau, Tennessee: a detailed analysis of broadband teleseismic P waveforms." J. Geophys. Res., 89 (1984), 7783-7795.

Ramesh, D.S., Kind, R., Yuan, X. "Receiver function analysis of the North American crust and upper mantle." Geophys. J. Int., 150 (2002), 91-108.

Saleeby, J.C. "Ocean floor accretion and volcano-plutonic arc evolution of the Mesozoic Sierra Nevada." The geotectonic development of California, Englewood Cliffs, New Jersey, 130-181.

Saleeby, J., Ducea, M., Clemens-Knott, D. "Production and loss of high-density batholithic root, southern Sierra Nevada California." Tectonics, 22 (2003), 1064-1086.

Schweichert, R.A., Cowen, D.S. "Early Mesozoic tectonic evolution of the western Sierra Nevada, California." Geol. Soc. America Bull., 86 (1975), 1329-1336.

Sedlock, R., "Geology and tectonics of the Baja California peninsula and adjacent areas." Geol. Soc. Of Amer., Special Paper 374 (2003), 1-42.

Shearer, P.M. "Seismic imaging of upper-mantle structure with new evidence for a 520-km discontinuity." Nature, 344 (1990), 121-126.

Sheffels, B., McNutt, M., "Role of Subsurface Loads and Regional Compensation in the Isostatic Balance of the Transverse Ranges, California: Evidence for intracontinental Subduction" J. Geophy. Res., 91 (1986), 6419-6431.

Simmons, N.A. "Imaging the mantle beneath southern California using receiver functions." Masters Thesis, Texas Tech University (2000).

Simmons, N.A. and Gurrola, H. "Multiple seismic discontinuities near the base of the transition zone in the Earth's mantle." Nature, 405 (2000), 13595-13609.

Spencer, J.E. "Uplift of the Colorado Plateau due to lithosphere attenuation during Laramide low-angle subduction." Jour. Geophys. Res., 101 (1996), 13595-13609.

Stewart, John H. "Basin-range structure in western North America: A review." Geol. Soc. America Mem., 152 (1977), 1-31.

Vacher, P., Mocquet, A., Sotin, C. "Computation of seismic profiles from mineral physics: the importance of the non-olivine components for explaining the 660 km depth discontinuity." Phys. Earth Planet. Inter., 106 (1998), 275-298.

Van der lee, S. and Nolet, G. "Upper mantle S-velocity structure of North America." J. Geophys. Res., 102 (1997), 22815-22838.

Vinnek, L. P., "Detection of waves converted from P-to-SV in the mantle." Phys. Earth Planet. Inter., 15 (1977), 294-303.

Xie, S. "Constraints on mantle structure from geochemistry, seismology, and mixing studies." Doctoral Thesis, University of California, Los Angeles, (2003).

PERMISSION TO COPY

In presenting this thesis in partial fulfillment of the requirements for a master's degree at Texas Tech University or Texas Tech University Health Sciences Center, I agree that the Library and my major department shall make it freely available for research purposes. Permission to copy this thesis for scholarly purposes may be granted by the Director of the Library or my major professor. It is understood that any copying or publication of this thesis for financial gain shall not be allowed without my further written permission and that any user may be liable for copyright infringement.

Agree (Permission is granted.)

_____ _____

Student Signature Date

Disagree (Permission is not granted.)

_____ _____

Student Signature Date